# Wireless Energy Harvesting for Autonomous Reconfigurable Intelligent Surfaces

Konstantinos Ntontin, *Member, IEEE*, Alexandros–Apostolos A. Boulogeorgos, *Senior Member, IEEE*, Emil Björnson, *Fellow, IEEE*, Wallace Alves Martins, *Senior Member, IEEE*, Steven Kisseleff, *Senior Member, IEEE*, Sergi Abadal, *Member, IEEE*, Eduard Alarcón, *Senior Member, IEEE*, Anastasios Papazafeiropoulos, *Senior Member, IEEE*, Fotis I. Lazarakis, and Symeon Chatzinotas, *Senior Member, IEEE*

***Abstract*—In the current contribution, we examine the feasibility of fully-energy-autonomous operation of reconfigurable intelligent surfaces (RIS) through wireless energy harvesting (EH) from incident information signals. Towards this, we first identify the main RIS energy-consuming components and present a suitable and accurate energy-consumption model that is based on the recently proposed integrated controller architecture and includes the energy consumption needed for channel estimation. Building on this model, we introduce a novel RIS architecture that enables EH through RIS unit-cell (UC) splitting. Subsequently, we introduce an EH policy, where a subset of the UCs is used for beamsteering, while the remaining UCs absorb energy. In particular, we formulate a subset al.ocation optimization problem that aims at maximizing the signal-to-noise ratio (SNR) at the receiver without violating the RIS's energy consumption demands. As a problem solution, we present low-complexity heuristic algorithms. The presented numerical results reveal the feasibility of the proposed architecture and the efficiency of the presented algorithms with respect to both the optimal and very high-complexity brute-force approach and the one corresponding to random subset selection. Furthermore, the results reveal how important the placement of the RIS as close to the transmitter as possible is, for increasing the harvesting effectiveness.**

***Index Terms*—Reconfigurable intelligent surfaces, autonomous operation, simultaneous energy harvesting and beamsteering, unit-cell splitting architecture.**

Manuscript received 21 April 2022; revised 31 July 2022; accepted 15 August 2022. Date of publication 24 August 2022; date of current version 15 February 2023. This work was supported in part by the Luxembourg National Research Fund (FNR) through the CORE Project RISOTTI under Grant 14773976; in part by the European Commission's Horizon 2020 Research and Innovation Programme (ARIADNE) under Grant 871464; and in part by the Digital Futures center. The editor coordinating the review of this article was Y. Hong. *(Corresponding author: Konstantinos Ntontin.)*

Konstantinos Ntontin, Wallace Alves Martins, Steven Kisseleff, and Symeon Chatzinotas are with the SnT, University of Luxembourg, 1855 Luxembourg City, Luxembourg (e-mail: kostantinos.ntontin@uni.lu; wallace.alvesmartins@uni.lu; steven.kisseleff@uni.lu; symeon.chatzinotas@uni.lu).

Alexandros–Apostolos A. Boulogeorgos is with the Department of Electrical and Computer Engineering, University of Western Macedonia, 50131 Kozani, Greece, and also with the Department of Digital Systems, University of Piraeus, 18534 Piraeus, Greece (e-mail: al.boulogeorgos@ieee.org).

Emil Björnson is with the Department of Electrical Engineering, Linköping University, 58183 Linköping, Sweden, and also with the Department of Computer Science, KTH, 10044 Kista, Sweden (e-mail: emilbjo@kth.se).

Sergi Abadal and Eduard Alarcón are with the NaNoNetworking Center in Catalunya, Universitat Politécnica de Catalunya, 08034 Barcelona, Spain (e-mail: abadal@ac.upc.edu; eduard.alarcon@upc.edu).

Anastasios Papazafeiropoulos is with the Communications and Intelligent Systems Research Group, University of Hertfordshire, Hatfield AL10 9AB, U.K., and also with the SnT, University of Luxembourg, 1855 Luxembourg City, Luxembourg (e-mail: tapapazaf@gmail.com).

Fotis I. Lazarakis is with the Wireless Communications Laboratory of the Institute of Informatics and Telecommunications, National Centre for Scientific Research–"Demokritos," 15341 Athens, Greece (e-mail: flaz@iit.demokritos.gr).

Digital Object Identifier 10.1109/TGCN.2022.3201190

## I. Introduction

THE DATA traffic demands increase steadily and exponentially [1]. To prevent a possible capacity crunch, a key proposed solution is traffic offloading to higher frequency bands [2]. More specifically, a large fraction of the traffic in future access networks is expected to utilize the millimeter-wave (mmWave) spectrum due to the larger available bandwidth [3]. However, this advantage comes with a cost: mmWave bands are more susceptible to fixed and moving blockages in comparison to their sub-6-GHz counterparts due to the high penetration loss that may even reach 40 dB for certain materials, such as tinted glass [4].

A possible solution to the blockage problem that has extensively been discussed in the literature is the creation of alternative signal paths through relays or passive reflectors. Relays can undoubtedly enhance the coverage by enabling the transmitted signal to be rerouted through them when the direct link is blocked. However, since relays require power amplifiers and possibly baseband processing, their power consumption will be comparable to that of mmWave small-cell base stations. This fact makes their massive deployment in mmWave networks questionable [5]. On the other hand, passive reflectors can enhance the coverage in mmWave networks, while requiring no power supply [5], [6]. However, the shape of the reflected signal is determined when they are deployed (e.g., based on Snell's law for a planar homogeneous reflector), and thus it cannot be adapted based on user mobility or changes in the propagation environment.

To circumvent the aforementioned limitations of relays and passive reflectors, reconfigurable intelligent surfaces (RISs) have been identified as possible countermeasures [7], [8]. RISs are artificial structures that usually consist of a dielectric substrate, which embeds conductive elements named unit cells (UCs), of sub-wavelength size and spacing. Typical UCs are composed of dipoles, patches, and string resonators.

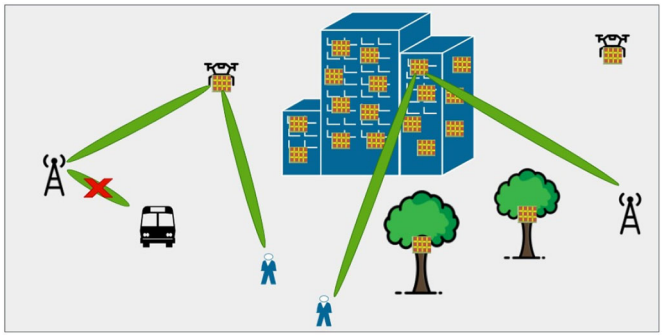

Fig. 1. Indicative scenarios in which autonomous RIS operation is desirable.

By properly tuning their impedance through semiconductor components, such as positive-intrinsic-negative (PIN) diodes, field-effect transistors (FETs), and radio-frequency micro-electromechanical systems (RF-MEMS), the amplitude and phase response to an impinging electromagnetic wave can be altered [9]. In particular, through such adjustment, different functionalities can be performed: beam steering toward a desired angular direction or toward a desired point, beam splitting, and absorption. In terms of power consumption, an amount of power is consumed for their reconfigurability, which arguably is significantly lower compared to relays' energy consumption, at least if the duty cycle of reconfiguration is low [8]. This has led to the characterization of RISs as nearly passive structures [10], [11].

Building on the above considerations, in this paper we examine the case for *autonomous RIS operation*, which we define as a mode, where the RIS does not require a dedicated power supply. Such a functionality has been suggested as a future potential in [12]. In terms of importance, there are various scenarios where the autonomous feature would be highly desirable. Such scenarios are depicted in Fig. 1. In particular, power-grid unavailability and aesthetics issues might prevent the deployment of RISs onto particular objects, such as trees. In addition, due to aesthetics reasons it could be difficult to acquire permissions from the building managers to deploy exterior cables onto the facades for powering the RISs. Supplying their energy needs through batteries that are not recharged perpetually by some gridless process is also not a viable option, since they would need constant monitoring and manual replacement. Finally, in the case of RISs equipping unmanned aerial vehicles (UAVs), supplying their energy needs through the vehicle batteries remains challenging, as it would drain them faster and reduce their flight time.

As far as related works on autonomous RISs are concerned, few recent works have started incorporating this requirement, either through time-splitting [13], [14], UC splitting [15], [16], or in a hybrid fashion [17]. In the time-splitting case, dedicated disjoint time intervals are allocated for either energy harvesting or information transmission, whereas in the unit-cell splitting one there is a common time interval for both energy harvesting and information transmission by devoting a subset of UCs for energy harvesting through absorption and its complement orthogonal subset for information transmission through reflection.

*Motivation and contribution:* For the control network, the mentioned works on energy-autonomous RIS operation consider the conventional separated field-programmable gate array (FPGA). However, it is widely argued that such architectures are usually bulky and suffer from significant energy consumption that render the possibility for autonomous operation highly questionable [12]. In addition, no evaluation has been performed regarding the plausibility of satisfying the RIS energy consumption demands through wireless energy harvesting in a practical scenario that incorporates user mobility. Motivated by this, the technical contribution of this work is as follows:

- We firstly identify the main RIS power-consuming modules and introduce the considered in this work energy consumption model that is based on the novel *integrated architecture* [12]. In addition, in contrast to existing works on autonomous RISs, the considered energy consumption model includes the energy burden for channel estimation.
- We present a novel RIS architecture that allows energy harvesting through suitable UC allocations, i.e., a subset of the UC can be used for energy harvesting, while the rest for beam steering, and derive closed-form expressions for the end-to-end signal-to-noise ratio (SNR) and direct current (DC) harvested power.
- Building on the aforementioned expressions, we formulate an optimization problem that outputs sets of UCs that need to be used for harvesting and beamsteering. The problem targets the maximization of the SNR at the end-user while concurrently satisfying the RIS's energy-consumption demands. In addition, due to the high complexity of the brute force approach (exhaustive search), we provide a low-complexity heuristic algorithms for its solution and prove that, under particular propagation conditions, some of the policies deliver the optimal subset al.ocation. Furthermore, for the particular policies we provide analytical expressions for the SNR statistics.
- We further comment on the advantages and disadvantages of the examined UC-splitting approach with its time-splitting conventional counterpart by presenting the corresponding formulas in the latter case.
- To validate the efficiency of the proposed algorithms, we perform extensive Monte-Carlo simulations and compare their performance against both the brute-force approach and the random subset selection.

The rest of this work is structured as follows.[1] In Section II, the system and channel models are presented together with the identification of the main RIS modules that consume power and the resulting power-consumption model. In Section III, the instantaneous DC harvested power and the end-to-end SNR are computed and the optimization problems of interest is formulated. In Section IV, heuristic algorithms for the solution

[1]This work is an extension of [18]. In particular, in [18] instead of an arbitrary fading model that we consider in this work, which makes the analysis more flexible and gives rise to our proposed algorithms, the special-case of free-space propagation is considered for both the transmitter-RIS and RIS-receiver links.

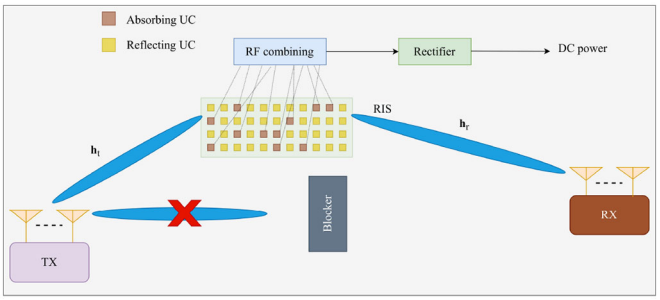


Fig. 2. Scenario and energy-harvesting architecture.

of the problem are provided and their complexity comparison with respect to the brute-force approach is assessed. Numerical results substantiate the effectiveness of the proposed low-complexity algorithms in Section V and, finally, Section VI concludes this work.

## II. System and RIS Power-Consumption Models

In this section, we first present the system model under consideration. Subsequently, we identify the power-consuming RIS modules and, based on them, we introduce the corresponding RIS power-consumption model.

### A. System Model

*1) Scenario:* As illustrated in Fig. 2, we consider a scenario in which a fixed transmitter (TX), such as a small-cell base station communicates with a mobile receiver (RX) through a planar RIS located in the far-field of both the TX and RX. The TX-RIS link, of distance $d_t$ m, and RIS-RX link, of distance $d_r$ m, constitute an alternative path to the direct TX-RX link that is assumed to be blocked. Furthermore, we assume that there is optical visibility of the RIS from both the TX and RX.[2] The RIS is a rectangular uniform planar array consisting of $M_s = M_x \times M_y$ UCs of size $d_x \times d_y$. $M_x$ $(M_y)$ and $d_x$ $(d_y)$ denote the number of UCs and their length in the x-axis (y-axis), respectively.

*2) Energy-Harvesting Architecture:* Among the $M_s$ UCs, $M_h$ UCs are configured to act as perfect absorbers of the impinging electromagnetic energy, which is used for supplying the RIS modules. Furthermore, we consider a corporate-feed network approach in which the radio frequency (RF) harvested power of the harvesting UCs is combined and driven to a single rectifier circuit through the particular network [19], [20]. The benefit of such an approach, compared to a solution in which a rectifier is attached to each UC and, subsequently, the DC harvested powers are combined, is the maximization of the input RF power at the RF circuit together with the minimization of the circuitry required for rectification. The former could be an essential requirement since the harvested power of a single UC might be low for turning on the diode of the rectifying circuit in an approach where such a circuit is attached to each UC. On the other hand, combining the harvested RF powers through the network could result in lower radiation to alternative current radiation efficiency compared to the one rectifier-per-UC approach [21]. The remaining $M_r = M_s - M_h$ UCs, are configured to act as perfect reflectors of the impinging energy, beamforming it toward the RX.

*3) TX and RX Antennas:* We assume that both the TX and RX are equipped with rectangular uniform planar arrays. In the TX (RX) case the number of antennas in the x-axis is denoted by $M_{t_x}$ $(M_{r_x})$ and the corresponding one in the y-axis by $M_{t_y}$ $(M_{r_y})$. In addition, the distance between adjacent antennas in the x-axis is denoted by $d_{t_x}$ $(d_{r_x})$ and the corresponding one in the y-axis by $d_{t_y}$ $(d_{r_y})$. In such a case, for the TX antenna by denoting the azimuth and elevation angles as $\phi$ and $\theta$, respectively, and assuming that the phase of its elements is adjusted so that the main lobe is directed to $(\theta_0, \phi_0)$, for its directivity, which we denote by $D_t(\theta, \phi)$, it holds [22]

$$D_t(\theta,\phi) = \frac{|g_t(\theta,\phi)|^2 |f(\theta,\phi)|^2}{M_{t_x} M_{t_y} R_t}, \tag{1}$$

where $g_t(\theta, \phi)$ and $f(\theta, \phi)$ are the array and element factors, respectively. It holds [22]

$$g_t(\theta,\phi) = \sum_{n=0}^{M_{t_x}} e^{-jn\left(\frac{2\pi}{\lambda} d_{t_x} \sin\theta\cos\phi - \frac{2\pi}{\lambda} d_{t_x} \sin\theta_0 \cos\phi_0\right)} \times \sum_{l=0}^{M_{t_y}} e^{-jl\left(\frac{2\pi}{\lambda} d_{t_y} \sin\theta\sin\phi - \frac{2\pi}{\lambda} d_{t_y} \sin\theta_0 \sin\phi_0\right)}. \tag{2}$$

In addition, [22] provides various formulas for $|f(\theta, \phi)|^2$, according to the considered antenna type. For instance, for parallel dipoles it holds

$$|f(\theta,\phi)|^2 = 1 - \sin^2\theta\cos^2\phi. \tag{3}$$

Finally,

$$\begin{aligned} R_t = s_0 &+ \sum_{r=1}^{M_{t_x}-1} \cos\left(r\frac{2\pi}{\lambda} d_{t_x} \sin\theta_0\cos\phi_0\right) \\ &\times \left(1 - \frac{r}{M_{t_x}}\right)(a_1 \sin A + a_2 \cos A) \\ &+ \sum_{q=1}^{M_{t_y}-1} \cos\left(q\frac{2\pi}{\lambda} d_{t_y} \sin\theta_0\sin\phi_0\right) \\ &\times \left(1 - \frac{q}{M_{t_y}}\right)(b_1 \sin B + b_2 \cos B) \\ &+ \sum_{r=1}^{M_{t_x}-1} \sum_{q=1}^{M_{t_y}-1} \cos\left(r\frac{2\pi}{\lambda} d_{t_x} \sin\theta_0\cos\phi_0 + q\frac{2\pi}{\lambda} d_{t_y} \sin\theta_0\sin\phi_0\right) \\ &\times \left(1 - \frac{r}{M_{t_x}}\right)\left(1 - \frac{q}{M_{t_y}}\right) \\ &\times (c_1 \sin C + c_2 \cos C), \end{aligned} \tag{4}$$

where

$$A = r\frac{2\pi}{\lambda} d_{t_x}, \quad B = q\frac{2\pi}{\lambda} d_{t_y}, \quad C = \sqrt{A^2 + B^2}. \tag{5}$$

[2]Such an assumption is justified by the normally high elevation of and RIS that is expected with respect to the TX and RX antennas.

The parameters $s_0\, a_1, a_2, b_1, b_2, c_1, c_2$ are given by [22, Table 1]. For simplicity and without a loss of generality, in this work we consider the case of isotropic antennas at the TX and RX. Hence, it holds $|f(\theta,\phi)|^2 = 1$ and $s_0 = 0.5$ $a_1 = 1/A$, $a_2 = 0$, $b_1 = 1/B$, $b_2 = 0$, $c_1 = 2/C$, $c_2 = 0$. $D_r(\theta,\phi)$ is given by the same formulas used for the computation of $D_t(\theta,\phi)$ after replacing $M_{t_x}$, $M_{t_y}$, $d_{t_x}$, and $d_{t_y}$ with $M_{r_x}$, $M_{r_y}$, $d_{r_x}$, and $d_{r_y}$, respectively. Finally, the gains of the TX and RX antennas, which we denote by $G_t(\theta,\phi)$ and $G_r(\theta,\phi)$, respectively, are given by $G_t(\theta,\phi) = \epsilon_t D_t(\theta,\phi)$ and $G_r(\theta,\phi) = \epsilon_r D_r(\theta,\phi)$, where $\epsilon_t$ and $\epsilon_r$ are the efficiencies of the TX and RX antennas, respectively.

*4) Channel Model:* We assume a flat-fading[3] channel model where the complex envelope channel vectors of the TX-RIS and RIS-RX links, denoted by $\mathbf{h}_t$ and $\mathbf{h}_r$, are given by

$$\mathbf{h}_t = \begin{bmatrix} h_{t_1} & \cdots & h_{t_{M_s}} \end{bmatrix}^T,\ \mathbf{h}_r = \begin{bmatrix} h_{r_1} & \cdots & h_{r_{M_s}} \end{bmatrix}^T, \quad (6)$$

where the UCs can be indexed arbitrarily. These vectors describe the joint effect of antenna gains, geometric pathloss, and multipath fading (i.e., the combination of small-scale and large-scale fading). In addition, we note that $\mathbf{h}_t$ and $\mathbf{h}_r$ are one-dimensional in spite the fact that both the TX and RX are equipped with multiple antennas. This holds under the assumption of the TX and RX antennas being phase aligned with the direction of the RIS since we assume that both the TX-RIS and RIS-RX links are subject to LoS conditions, owing to the optical visibility.

The channel vectors $\mathbf{h}_\mathrm{t}$ and $\mathbf{h}_\mathrm{r}$ are time-varying due to mobility and multipath fading, which calls for a time-varying RIS configuration. We consider a block-fading model where the channel vectors are fixed within fixed-size time intervals, but change abruptly between intervals. Hence, the RIS must be reconfigured in each interval. The duration of these intervals depends on the time-variation of the channel. The optimization problems and policies developed in this article operate on a per-interval basis, thus they can be applied irrespective of how the channel realizations are generated. For example, a stationary fading distribution such as Rayleigh, Nakagami-m, Weibull, or Rice could be used, but also a deterministic ray-traced or measured channel evolution could be considered.

*5) Frame Structure and Channel Estimation:* As far as the frame structure is concerned, which determines the energy consumption needs of the RIS, each frame that has a fixed duration of $N_\mathrm{fr}$ time slots comprises the signaling period of duration $N_\mathrm{sl}$ slots, which is used for tasks such as time and carrier frequency synchronization together with channel estimation. Regarding the latter, in this work we assume that channel estimation is realized in each signaling period even if the signal quality at the RX does not dictate the need for channel estimation. Such a protocol is consistent with the operation of current standards, such as the Long Term Evolution, in which continuously there is channel estimation performed in dedicated resource elements during the transmissions of resource blocks. The signaling period is followed by the payload period of duration $N_\mathrm{pl}$ time slots in which simultaneously the RIS harvests energy by the allocated $M_h$ UCs and performs information transmission through beamforming towards the RX by the remaining $M_r$ UCs. The corresponding frame structure is depicted in Fig. 3.

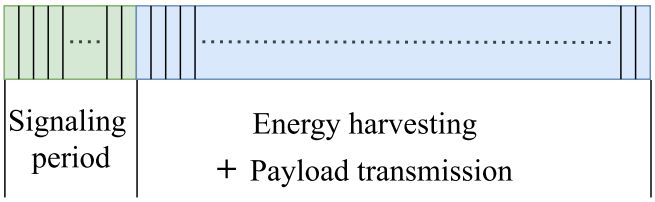


Fig. 3. Frame structure.

*6) Channel Estimation Protocol:* In order to maintain a low-complexity RIS structure suitable for autonomous operation, we assume that neither channel estimation can be performed in the RIS, due to lack of the required circuitry, nor pilot signals can be sent by the RIS to the TX and RX for channel estimation of the individual TX-RIS and RIS-RX links. Instead, we assume that estimation of the cascaded Tx-RIS-RX links can be performed at the TX through pilots sent by the RX.[4] For the estimation of the cascaded TX-RIS-RX links we consider the protocol presented in [26]. In particular, at any given time slot during the channel estimation phase only one of the $M_s$ RIS UCs is activated and it is in ON mode, while the rest are in the OFF mode, and the process is performed until all the cascaded links are estimated.[5] Hence, the maximum number of time slots required for channel estimation is equal to $M_s$ in the case that all the UCs are used in the process.[6] This means that $M_s \leq N_\mathrm{sl}$ should hold.

After obtaining the cascaded TX-RIS-RX links, the individual TX-RIS and RIS-RX links can be estimated through the method of [29] that is based on eigenvalue decomposition. For simplicity and since our focus is not on channel estimation, in this work we assume that a perfect knowledge of the TX-RIS and RIS-RX links can be acquired through the aforementioned approach. Let us note that in the considered scenario the channel knowledge of the individual TX-RIS link is essential so that the maximum amount of energy is absorbed by the UCs that act as absorbers. This is achieved after properly adjusting their impedance response, according to the particular channel estimates.

[3]The flat fading assumption can hold even in the large-bandwidth case of mmWave and THz links due to the very small delay spreads associated with highly directional transmissions [23] or due to a negligible effect of the inter-symbol interference by optimizing the RIS phase shifts with respect to the strongest tap of the channel (line-of-sight (LoS) component) [24].

[4]Assuming that in practice it would be more realistic that the TX estimates the cascaded channel instead of the RX since the TX is the fixed base station and the RX the device of the mobile user. In addition, such a consideration presupposes that the channel reciprocity for the TX-RIS-RX channel holds. This has experimentally been tested to hold under certain conditions [25].

[5]As it is described in [27], the state OFF of a UC means that there is only structure-mode reflection generated as if the element is a conducting object, whereas the state ON means that there are both structure-mode reflection and antenna-mode reflection.

[6]If the TX-RIS channel is sparse, a smaller number than $M_s$ UCs to be turned ON might be sufficient for adequately accurate channel estimation. In such a case, compressive sensing can be leveraged to obtain the corresponding channel knowledge related to the remaining UCs that are not turned ON [28].

*Remark 1:* As we understand from the considered channel estimation protocol, although the RIS is not equipped with active components that would enable it to perform channel estimation on it, still an amount energy is consumed at the RIS due to its reconfigurations needed so that channel estimation is effectively performed at the TX (small-cell base station) through pilot signaling from the RX (mobile user).

In addition, even if the maximum amount of $M_s$ time slots is required for channel estimation during the signaling phase, the assumption of a block fading channel, where the channel remains stationary in the duration of a frame, can still hold even for large RIS sizes. For instance, by assuming that the RX is moving with the average pace of a person that is equal to 1.4 m/s the channel coherence time as the inverse of Doppler spread is equal to 7.7 ms for a 28 GHz carrier. By assuming single-carrier modulation that has shown to exhibit a superior performance compared with orthogonal frequency-division multiplexing, the symbol duration (time-slot duration) is equal to 2.44 ns for a signal bandwidth of 500 MHz and a roll-off factor of 0.22 [30]. If, for instance, $N_{\mathrm{sl}} = 1000$, which is a value that can accommodate the channel estimation of a large RIS up to 1000 UCs, and the signaling period is 10% of the frame duration, 770 consecutive transmitted frames are within the coherence time of the channel. This shows that the proposed channel estimation protocol in combination with single-carrier modulation can accommodate large RISs without the risk of falling outside the coherence time of the channel during the transmission of a frame.

### B. Power-Consumption Model

To present a suitable RIS energy consumption model, we firstly need to identify the main RIS power-consuming modules, namely: i) impedance-adjusting semiconductor components, ii) control network, and iii) rectifier. They are described below.

*1) Impedance-Adjusting Semiconductor Components:* The energy consumption of these components is characterized by static and dynamic factors. The static factor corresponds to their uninterrupted energy consumption due to leakage currents originating from the bias voltages when they operate in steady state. Usually, this factor is negligible for FETs and RF MEMS [31]. On the other hand, the dynamic factor constitutes a non-negligible factor related to the charging and discharging of internal capacitors during bias voltage level changes. This is needed for UC phase and amplitude response adjustment. It appears only when the semiconductor components change state.

*2) Control Network:* As described in [8], [12], the RIS needs to receive external commands regarding the new configuration states for the UCs. This can be achieved by one of the following basic approaches [12]: i) detached microcontroller architecture and ii) integrated architecture. The first one is the common architecture that has been used for several years in which the control network is realized by a microcontroller, such as an FPGA. Such architectures are usually bulky and subject to significant energy consumption, thus reducing the potential for RIS autonomous operation [12]. In contrast to the FPGA-based architectures, the control network in the integrated architecture is realized by a network of communicating chips (usually one per UC) that read the UC state and adjust the bias voltages of the impedance-adjusting semiconductor elements. These circuits receive, interpret, and apply the commands and exhibit their own static and dynamic energy consumption due to leakage and transistor switching, respectively [32]. In addition, they are likely to use asynchronous logic as it does not require a complex and power-hungry clock signal distribution [33]. Furthermore, it has been suggested that such chips could also operate autonomously through energy harvesting, based on nano-networking advancements [12], [34].

*3) Rectifier:* For the RF-to-DC power conversion that is needed to power the electronic modules of the RIS, a rectifier circuit follows the RF combiner. This circuit can be either passive that exhibits negligible energy consumption, or active, by incorporating active diodes with lower voltage drop that can increase the conversion efficiency [35]. In the latter case, the rectifier exhibits a non-negligible energy consumption.

To minimize the RIS energy consumption, we consider an integrated RIS architecture. Moreover, it is assumed that each UC is connected to one chip that controls and adjusts its impedance through an impedance-adjusting semiconductor component [32]. By assuming that only passive rectifiers are employed on the RIS and denoting its power consumption by $P_{\mathrm{RIS}}$, it holds that [36, eq. (4.5)]

$$P_{\mathrm{RIS}} = P_{\mathrm{st}}^{\mathrm{tot}} + P_{\mathrm{dyn}}^{\mathrm{tot}}, \tag{7}$$

where $P_{\mathrm{st}}^{\mathrm{tot}}$ and $P_{\mathrm{dyn}}^{\mathrm{tot}}$ denote the total static and dynamic RIS power consumption that incorporate the consumption arising from both the control chips and impedance-adjusting semiconductor components.

Regarding $P_{\mathrm{st}}^{\mathrm{tot}}$, under the assumption of one control chip and one impedance-adjusting semiconductor component per UC, it is expected to scale linearly with the number of UCs. Hence, we have

$$P_{\mathrm{st}}^{\mathrm{tot}} = M_s P_{\mathrm{st}}, \tag{8}$$

where $P_{\mathrm{st}}$ is the static power consumption associated with a single UC.

As far as $P_{\mathrm{dyn}}^{\mathrm{tot}}$ is concerned, it holds that

$$P_{\mathrm{dyn}}^{\mathrm{tot}} = P_{\mathrm{ce}}^{\mathrm{tot}} + P_{\mathrm{eh,pl}}^{\mathrm{tot}}, \tag{9}$$

where $P_{\mathrm{ce}}^{\mathrm{tot}}$ is the total power consumption related to the UC reconfigurations needed for channel estimation and $P_{\mathrm{eh,pl}}^{\mathrm{tot}}$ the power consumption related to the UC reconfigurations needed for both energy harvesting and information transmission through reflection.

Let us now denote the number of reconfiguration periods in a reference observation time $T$ with $N_{\mathrm{rec}}$. By denoting the duration of a frame by $T_{\mathrm{fr}}$, it holds that $N_{\mathrm{rec}} = \frac{T}{T_{\mathrm{fr}}}$ Furthermore, by approximately assuming that the energy consumption for a UC reconfiguration for either reflection or absorption is the same for all UCs and it is equal to $E_{\mathrm{UC}}$, it holds that [36, eq. (4.7)]

$$P_{\mathrm{ce}}^{\mathrm{tot}} = \frac{N_{\mathrm{rec}} M_s E_{\mathrm{UC}}}{T} = \frac{M_s E_{\mathrm{UC}}}{T_{\mathrm{fr}}} = \frac{M_s E_{\mathrm{UC}}}{N_{\mathrm{fr}} T_{\mathrm{slot}}} \tag{10}$$

and

$$P_{\text{eh,pl}}^{\text{tot}} = \frac{N_{\text{rec}} M_s E_{\text{UC}}}{T} = \frac{M_s E_{\text{UC}}}{T_{\text{fr}}} = \frac{M_s E_{\text{UC}}}{N_{\text{fr}} T_{\text{slot}}}, \quad (11)$$

where $T_{\text{slot}}$ is the time-slot duration. Equation (10) originates due to the fact that with the considered channel estimation protocol one-by-one the UCs are turned on for estimation. Hence, in one channel estimation period in total all the UCs of the RIS would be turned on. In addition, (11) originates due to the fact that after channel estimation the impedance of all UCs needs to be adjusted for either absorption or reflection, according to the channel estimates. Hence, based on the above we understand that the RIS reconfigurations needed for both channel estimation and simultaneous energy harvesting and payload transmission result in the same amount of energy/power consumed.

Hence, based on (8), (9), (10), and (11), (7) becomes

$$P_{\text{RIS}} = M_s \left( P_{\text{st}} + 2\frac{E_{\text{UC}}}{T_{\text{fr}}} \right). \quad (12)$$

*Remark 2:* According to (12), the RIS power consumption does not depend on the velocity of the RX. This comes in contrast with common claims in the literature that the power consumption of the RIS depends on how often it needs to reconfigure itself so to adapt to the channel varying conditions of a mobile user. That would hold only in the case where channel estimation follows a dynamic protocol in which channel estimation is initiated only when there is a substantial change in the received signal quality. However, this is not the principle under which current standards work. Instead, according to the considered protocol in this work the RIS needs to reconfigure itself at every frame for both channel estimation and subsequent UC impedance adjustment, based on the acquired estimates. This, as aforementioned, follows the working principle of known standards, such as the Long Term Evolution.

In addition, we note that $P_{\text{ce}}^{\text{tot}}$ can be considered as an upper bound on the RIS power consumption that is devoted to channel estimation since the amount of UCs that need to be turned on can be smaller than $M_s$ if the TX-RIS is sparse, as mentioned in Section II-A. As a result, also (12) gives an upper bound on the total RIS power consumption.

## III. DC Harvested Power, End-to-End SNR, and Problem Formulation

The aim of this section is to first present and quantify the autonomous RIS-empowered system design parameters and subsequently to use them to formulate the optimization problem of interest. In more detail, Section III-A returns a closed-form expression for the harvested power, Section III-B reports the end-to-end SNR and, finally, Section III-C describes the formulation of the optimization problem.

### A. DC Harvested Power

For the DC harvested power, we use the non-linear model from [37], which has been extensively validated through experimental measurements. According to this model, the output DC power of the rectifier can be evaluated as

$$P_{\text{DC}} = \frac{\frac{P_{\max}}{1+e^{-a(P_{\text{harv}}-b)}} - \frac{P_{\max}}{1+e^{ab}}}{1 - \frac{1}{1+e^{ab}}}, \quad (13)$$

where $P_{\text{harv}}$ is the RF power that is inputted to the rectifier and $P_{\max}$ is a constant denoting the maximum harvested power in the case that the harvesting circuit at the rectifier is saturated. In addition, $a$ and $b$ are circuit-specific parameters, which are related to the resistance, capacitance, and turn-on voltage of the diode used for rectification [37].

As far as $P_{\text{harv}}$ is concerned, let us denote the set of the UCs that are selected for energy harvesting by $\mathcal{A}_h$. Since the transmit power is $P_t$, the $i_{\text{th}}$ UC, $i \in \mathcal{A}_h$, will receive a signal $y_i = \sqrt{P_t} h_{t_i}$, where the thermal noise has been omitted since it cannot be harvested. Hence, the total harvested power as a function of $\mathcal{A}_h$ can be expressed as

$$P_{\text{harv}} = P_t \sum_{i \in \mathcal{A}_h} |h_{t_i}|^2. \quad (14)$$

We note that according to (14) only the power corresponding to the transmission from the TX is taken into account in the harvesting process. This is due to the assumption that the radiation pattern of the RIS corresponding to the harvesting UCs is aligned with the direction of the TX main lobe (that is directed toward the RIS center) in order to maximize the absorption of the power arriving from the particular direction. For this reason, it is expected that the absorbed power level of ambient signals arriving to the RIS from other directions would be negligible compared to the one arriving from the TX.

### B. End-to-End SNR

Let $\mathcal{A}_r$ denote the set of UCs that are selected for reflection, which is the orthogonal complement of $\mathcal{A}_h$, i.e., $\mathcal{A}_r = \mathcal{A}_h^C$. The end-to-end SNR $\gamma$ can be obtained by following the standard approach as [38], [39], [40]

$$\gamma = \frac{P_t}{\sigma^2} \left| \sum_{k \in \mathcal{A}_r} h_{t_k} h_{r_k} e^{j\left(\phi_k + \angle h_{t_k} + \angle h_{r_k}\right)} \right|^2, \quad (15)$$

where $\phi_k$ is the induced phase response from the $k_{\text{th}}$ UC, $\angle$ denotes the angle of the corresponding complex number, and $\sigma^2$ is the variance of the thermal noise at the RX, computed in dBm as $\sigma^2 = -174 + 10\log_{10}(W) + \mathcal{F}_{\text{dB}}$, where $\mathcal{F}_{\text{dB}}$ is the noise figure of the RX in dB and $W$ is the signal bandwidth in Hz. From (15) it is evident that the SNR is maximized by setting

$$\phi_k = -\angle h_{t_k} - \angle h_{r_k}, \text{ for } \quad \text{k} \in \mathcal{A}_{\text{r}}. \quad (16)$$

By substituting (16) in (15), the maximum SNR as a function of $\mathcal{A}_r$ can be written as

$$\gamma(\mathcal{A}_r) = \frac{P_t}{\sigma^2} \left( \sum_{k \in \mathcal{A}_r} |h_{t_k}||h_{r_k}| \right)^2. \quad (17)$$

We further note that setting the impedance of the UCs dedicated for beamsteering in a way that perfect reflection is

achieved with a phase response given by (16) indicates that independent tuning of the UC amplitude and phase response can be achieved. Although this, in general, does not hold and a level of inter-dependency between the UC amplitude and phase response is expected [41], there have been advanced literature designs considerably mitigating such a coupling effect [42], [43]. Hence, we can view (17) as an upper bound of the maximum SNR that can be achieved with more advanced RIS designs.

### C. Problem Formulation

The problem is formulated as

$$\begin{aligned} &\underset{\mathcal{A}_r}{\text{maximize}} \;\; \gamma(\mathcal{A}_r) \\ &\text{subject to} \;\; P_{\text{DC}}(\mathcal{A}_h) \geq P_{\text{RIS}}. \end{aligned} \tag{18}$$

Based on (13), (14), and (17), (18) can be rewritten as

$$\begin{aligned} &\underset{\mathcal{A}_r}{\text{maximize}} \;\; \left( \sum_{k \in \mathcal{A}_r} |h_{t_k}||h_{r_k}| \right)^2 \\ &\text{subject to} \;\; \frac{\frac{P_{\max}}{1+\exp\left(-a\left(\eta_{\text{RF}}\, P_t \sum_{i \in \mathcal{A}_h} |h_{t_i}|^2 - b\right)\right)} - \frac{P_{\max}}{1+e^{ab}}}{1 - \frac{1}{1+e^{ab}}} \geq P_{\text{RIS}}. \end{aligned} \tag{19}$$

The optimization problem of (19) is combinatorial and a solution in closed form does not exist in the general case where the channel gains $|h_{t_k}|$ and $|h_{r_k}|$ vary with $k$ due to multipath fading. The combinatorial nature means that a brute-force search approach (exhaustive search) is required to find the optimal $\mathcal{A}_r$ and $\mathcal{A}_h$. By denoting the number of possible combinations to be examined as $N_{\text{comb}}$, it holds that

$$N_{\text{comb}} = \sum_{l=1}^{M_s - 1} \binom{M_s}{l} = 2^{M_s} - 2. \tag{20}$$

Thus, $N_{\text{comb}}$ can be very large even for moderate $M_s$ and a brute-force approach is not viable in terms of execution time.[7] As a result, in Section IV we provide heuristic algorithms for solving the problem of substantially lower complexity.

*Remark 3:* Depending on the channel realization and $P_{\text{RIS}}$, the solution of (19) might not be feasible. In such cases, there can be different approaches of how the communication towards the RX can be realized. One possible solution is to have the RIS equipped with a battery that can be used in these urgent situations. Another approach is to harvest an amount of power that is higher than the RIS power consumption needs so that it can be used when the harvested power is lower than the particular needs. Additionally, as another alternative, the TX could switch to a sub-6 GHz band that is less susceptible to blockages compared with mmWave bands and realize the communication with the RX without the involvement of an RIS.[8]

[7]For instance, for $M_s = 25$ it holds that $N_{\text{comb}} = 33554430$.

[8]This would be doable considering that major telecom operators plan to use multiple bands for offering their 5G services [44].

**Algorithm 1** Ordering of the RIS-RX Link Channel Gains

1: Arrange $|h_{r_m}|$, $m = 1, 2, \ldots, M_s$, in descending order, i.e., $\left|h_{r_{(1)}}\right| \geq \left|h_{r_{(2)}}\right| \geq, \ldots, \geq \left|h_{r_{(M_s)}}\right|$.Set iteration index $i = 1$
2: **repeat** {Loop}
3: Set $\mathcal{A}_r = \left\{\mathcal{L}\left(\left|h_{r_{(1)}}\right|, \ldots, \left|h_{r_{(i)}}\right|\right)\right\}$, $\mathcal{A}_h = \left\{\mathcal{L}\left(\left|h_{r_{(i+1)}}\right|, \ldots, \left|h_{r_{(M_s)}}\right|\right)\right\}$
4: **until** Constraint in (19) is not satisfied for $i = i_s$
5: **Output** $\mathcal{A}_r = \left\{\mathcal{L}\left(\left|h_{r_{(1)}}\right|, \ldots, \left|h_{r_{(i_s-1)}}\right|\right)\right\}$, $\mathcal{A}_h = \left\{\mathcal{L}\left(\left|h_{r_{(i_s)}}\right|, \ldots, \left|h_{r_{(M_s)}}\right|\right)\right\}$

## IV. Proposed Algorithms and Complexity Comparison

### A. Proposed Algorithms

In this section, we first provide low-complexity heuristic algorithms for solving the considered problem. Subsequently, we prove that in the special case of equal-gain conditions in the TX-RIS link, some of the proposed algorithms deliver the optimal solution to the problem. Furthermore, for the particular algorithms we provide analytical expressions for the SNR statistics. Finally, we compare the time complexity of the brute-force approach with the corresponding one of the proposed algorithms.

By directly inspecting (19), we observe that the objective function to be maximized depends on both the TX-RIS and RIS-RX channel gains. Hence, at first a natural choice of heuristic algorithms that target the maximization of the utility function of (19) involves channel-gain ordering of either the RIS-RX links, or product of the TX-RIS and RIS-RX links, or TX-RIS links, and selection of the highest number of the respective UCs for beamsteering for which the constraint of (19) is satisfied. However, among the aforementioned 3 options, intuitively the last one that involves ordering of only the TX-RIS links is expected to perform poorly compared to the other 2 due to the TX-RIS links being also involved in the energy harvesting process. Hence, allocating the strongest TX-RIS links for maximizing the objective function of (19) inevitably leaves weaker TX-RIS links for satisfying the energy harvesting constraint. This, in turn, is expected to increase the number of UCs allocated for energy harvesting while at the same time reducing the ones allocated for reflection compared to the other 2 options, thus reducing the overall SNR. Due to this, we consider channel-gain ordering of either the RIS-RX links or the product of the TX-RIS and RIS-RX links. This reasoning gives rise to Algorithms 1 and 2 that are described as follows.

$\mathcal{L}(\cdot)$ denotes a function that takes as argument channel gains and returns as output the UC indices that correspond to the particular gains. In addition to Algorithms 1 and 2 that target the utility function of (19), it is also reasonable to target the constraint of (19). To this end, a rational approach is to maximize the number of UCs participating in beamsteering by minimizing the number of UCs dedicated for energy harvesting. The latter is achieved by dedicating for harvesting the

**Algorithm 2** Ordering of the Product of the TX-RIS and RIS-RX Link Channel Gains

1: Arrange $g_m = |h_{t_m}||h_{r_m}|$, $m = 1, 2, \ldots, M_s$, in descending order, i.e., $g_{(1)} \geq g_{(2)} \geq, \ldots, \geq g_{(M_s)}$. Set iteration index $i = 1$
2: **repeat** {Loop}
3: Set $\mathcal{A}_r = \left\{g_{(1)}, \ldots, g_{(i)}\right\}$, $\mathcal{A}_h = \left\{g_{(i+1)}, \ldots, g_{(M_s)}\right\}$
4: **until** Constraint in (19) is not satisfied for $i = i_s$
5: **Output** $\mathcal{A}_r = \left\{\mathcal{L}\left(g_{(1)}, \ldots, g_{(i_s-1)}\right)\right\}$, $\mathcal{A}_h = \left\{\mathcal{L}\left(g_{i_{(\text{stop})}}, \ldots, g_{(M_s)}\right)\right\}$

**Algorithm 3** Ordering of the TX-RIS Link Channel Gains

1: Arrange $\left|h_{t_m}\right|$, $m = 1, 2, \ldots, M_s$, in descending order, i.e., $\left|h_{t_{(1)}}\right| \geq \left|h_{t_{(2)}}\right| \geq, \ldots, \geq \left|h_{t_{(M_s)}}\right|$. Set iteration index $i = 1$
2: **repeat** {Loop}
3: Set $\mathcal{A}_r = \left\{\mathcal{L}\left(\left|h_{t_{(i+1)}}\right|, \ldots, \left|h_{t_{(M_s)}}\right|\right)\right\}$, $\mathcal{A}_h = \left\{\mathcal{L}\left(\left|h_{t_{(1)}}\right|, \ldots, \left|h_{t_{(i)}}\right|\right)\right\}$
4: **until** Constraint in (19) is not satisfied for $i = i_s$
5: **Output** $\mathcal{A}_r = \left\{\mathcal{L}\left(\left|h_{t_{\left(i_s^{(A)}+1\right)}}\right|, \ldots, \left|h_{t_{(M_s)}}\right|\right)\right\}$, $\mathcal{A}_h = \left\{\mathcal{L}\left(\left|h_{t_{(1)}}\right|, \ldots, \left|h_{t_{(i_s)}}\right|\right)\right\}$

UCs associated with the largest values of $|h_{t_m}|$, according to the proposed Algorithm 3 that is described as follows.

*Special case of equal-gain propagation in the TX-RIS link*: In this special case, we have $|h_{t_1}| = \cdots = |h_{t_{M_s}}|$, which means that the pathloss is the same between the TX and every UC. This condition is exactly satisfied in free-space far-field propagation, but can also be approximately occurring in other scenarios with a dominant LoS path (i.e., in Rician channels with large $K$-factor). Furthermore, we focus on the TX-RIS link for this case study since for fixed positions of the TX and RIS the TX-RIS link is expected to be dominated by a strong LoS component. This means that the propagation conditions in the TX-RIS links would be close to the ideal case of equal-gain propagation. This would arise in likely scenarios where the TX is a base station and the RIS is mounted on a fixed structure, such as a building. In this special case, we can prove the following proposition.

*Proposition 1:* Under equal-gain propagation in the TX-RIS link with $|h_{t_1}|^2 = \cdots = |h_{t_{M_s}}|^2 = \beta$, Algorithms 1 and 2 deliver the optimal selection of $\mathcal{A}_r$ and $\mathcal{A}_h$ with

$$i_s = M_s - \left\lceil \frac{-\left(\frac{1}{a}\right)\log\left(\frac{P_{\max}}{P_{\text{RIS}}\left(1-\frac{1}{1+e^{ab}}\right)+\frac{P_{\max}}{1+e^{ab}}} - 1\right) + b}{\eta_{\text{RF}} P_t \beta} \right\rceil + 1, \tag{21}$$

where $\lceil \cdot \rceil$ is the ceiling function. In addition, the resulting cumulative density function (CDF) of Algorithms 1 and 2 that is denoted by $F_{\gamma_{\text{eq}}}(\gamma)$ can be approximated by

$$F_{\gamma_{\text{eq}}}(\gamma) \cong 2^{1-C} e^{Q/2} \sum_{m=0}^{C} \binom{C}{m} \sum_{l=0}^{m+V} (-1)^l s_l \times \mathbb{R}\left[ m_{h_r}\left(\frac{Q + j2\pi l}{2\sigma\sqrt{\frac{\gamma}{P_t\beta}}}\right) / (Q + j2\pi l) \right], \tag{22}$$

where

$$m_{h_r}(s) = (i_s - 1)\binom{M_s}{i_s - 1} \int_0^{\frac{\pi}{2}} e^{-s\tan\theta} f_{h_r}(\tan\theta) \times [1 - m(0, \tan\theta)]^{M_s - i_s + 1} m(s, \tan\theta)^{i_s - 2} \sec\theta^2 d\theta \tag{23}$$

with

$$m(s, x) = \int_x^{\infty} e^{-st} p(t)\, dt. \tag{24}$$

Furthermore, it holds that $s_0 = 0.5$, $s_l = 1$ for any $l \geq 1$, and $C$, $V$, and $Q$ are constants. Moreover, $f_{h_r}(x)$ denotes the probability density function of $|h_{r_m}|$, $m = 1, 2, \ldots, M_s$.

*Proof:* The proof is given in the Appendix. ■

The range of values of $C$, $V$, and $Q$ for which $F_{\gamma_{\text{eq}}}(\gamma)$ is computed with a good accuracy depends on the statistics of $|h_{r_m}|$.[9] In addition, we observe that if $m(s, x)$ can be computed in closed form, $F_{\text{eq}}(\gamma)$ involves only a single integral, which notably reduces the complexity for its computation. Finally, we note that the higher the deviation of the propagation conditions in the TX-RIS link is with respect to equal-gain propagation, the higher the performance gap between the brute-force approach and Algorithms 1 and 2 is expected to be. This will be verified in the numerical results of Section V.

### B. Time Complexity

The time complexity of the brute-force approach, which we denote by $C_{\text{bf}}$, is given by

$$C_{\text{bf}} = \mathcal{O}(N_{\text{comb}}) = \mathcal{O}\left(2^{M_s} - 1\right). \tag{25}$$

As far as the proposed heuristic algorithms are concerned, they all rely on numerical sorting and, hence, they exhibit the same time complexity. This consists of two parts. The first part is related to the complexity associated with the numerical sorting. By using, for instance, the heapsort algorithm [46], the time complexity for numerical sorting of Algorithms 1, 2, 3 scales with $M_s \log(M_s)$. The second part is related to the search required until the solution is reached for the 3 algorithms, In the worst case scenario, the algorithms reach a solution after $M_s - 1$ searches, hence their time complexity scales with $M_s - 1$ as an upper bound. As a result, for the total time complexity of the proposed algorithms, which we denote by $C_{\text{al}}$, it holds that

$$C_{\text{al}} = \mathcal{O}(M_s \log(M_s) + M_s - 1). \tag{26}$$

To substantiate, the computational advantage of the proposed algorithms with respect to the brute-force approach,

[9] In [45] the authors find that the values $Q = 30$, $V = 18$, and $C = 24$ give a good accuracy for Rician channels.

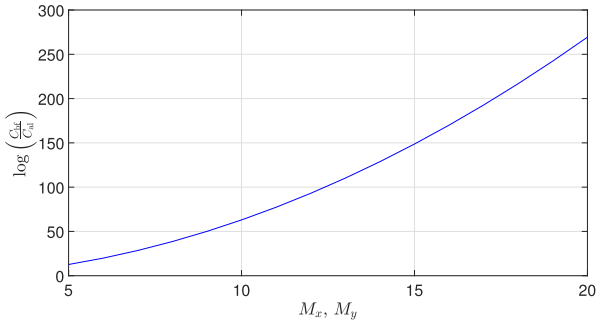


Fig. 4. Time-complexity comparison versus the number of the RIS UCs.

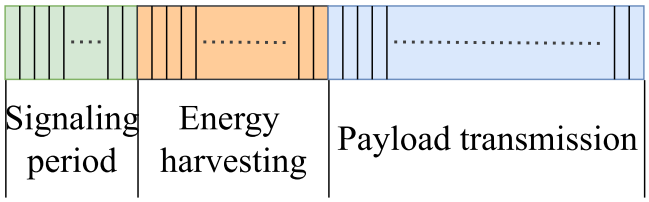


Fig. 5. Frame structure in the time-splitting case.

in Fig. 4 we illustrate the logarithm of the ratio of the number of computations needed for the brute-force approach over the corresponding one of the proposed algorithms versus the number of RIS elements assuming $M_x = M_y$. As we observe from Fig. 4, the computational benefit of the proposed algorithms with respect to brute force substantially increases for increasing number of RIS elements.

### C. Comparison With the Time-Splitting Approach

Let is now examine how the proposed UC-splitting approach for energy harvesting compares with the traditional time-splitting approach. The latter protocol, as it is presented in [13], [14], employs a dedicated time interval to energy harvesting during the frame structure in which all the UCs act as absorbers. This interval is followed by the payload transmission interval where all the UCs act as reflectors for beamforming the impinging wave towards the RX. The mentioned frame structure is depicted in Fig. 5. The number of time slots devoted to energy harvesting is denoted by $N_h$.

As far as the power consumption of the time splitting protocol with respect to its UC-splitting counterpart is concerned, after the signaling period and the estimation of the channel coefficients a reconfiguration period is needed to adjust the impedance of all the UCs so that they act as perfect absorbers and another one during the payload transmission period so that they act as perfect reflectors. Consequently, the dynamic power consumption in the time-splitting protocol is larger by $\frac{N_{\text{rec}} M_s E_{\text{UC}}}{T}$ with respect to the UC-splitting one. Hence, by denoting the RIS power consumption in the time-splitting case by $P_{\text{RIS}}^{\text{TS}}$, it holds

$$P_{\text{RIS}}^{\text{TS}} = M_s \left( P_{\text{st}} + 3 \frac{N_{\text{rec}} E_{\text{UC}}}{T} \right) = M_s \left( P_{\text{st}} + 3 \frac{E_{\text{UC}}}{T_{\text{fr}}} \right) \quad (27)$$

On the other hand, the SNR during the payload transmission is larger in the time-splitting case since all the UCs are used for beamforming towards the RX. By denoting it as $\gamma^{\text{TS}}(\mathcal{A}_r)$, it holds

$$\gamma^{\text{TS}}(\mathcal{A}_s) = \frac{P_t}{\sigma^2} \left( \sum_{k=1}^{M_s} |h_{t_k}||h_{r_k}| \right)^2, \quad (28)$$

where $\mathcal{A}_s$ denotes the set of all the UCs, i.e., $\mathcal{A}_s = \mathcal{A}_h \cup \mathcal{A}_r$.

From the frame structure depicted in Fig. 5 we observe that in the time-splitting protocol the RIS harvests energy for $\frac{N_h}{N_{\text{fr}} - N_{\text{sl}}}$ of the respective time of its UC-splitting counterpart. Hence, considering that the resulting SNR is always the maximum achievable in the time-splitting case, the equivalent formulation of (18) concerns only the minimization of $N_h$ so that the payload transmission time is maximized. Hence, we have

$$\begin{aligned} &\underset{N_h}{\text{minimize}} \quad N_h \\ &\text{subject to} \quad \frac{N_h}{N_{\text{fr}} - N_{\text{sl}}} P_{\text{DC}}(\mathcal{A}_s) \geq P_{\text{RIS}}^{\text{TS}}. \end{aligned} \quad (29)$$

Equation (29) has the following closed-form solution, denoted by $N_h^*$

$$N_h^* = \left\lceil \frac{(N_{\text{fr}} - N_{\text{sl}}) P_{\text{RIS}}^{\text{TS}}}{P_{\text{DC}}(\mathcal{A}_s)} \right\rceil. \quad (30)$$

*Remark 4:* Form the above we understand that the time-splitting protocol results in a higher energy consumption than its UC counterpart. On the other hand, time splitting results in the highest achievable SNR due to the participation of all the UCs in beamforming towards the RX. In addition, it does not incur any time complexity for the optimal allocation of resources to energy harvesting (computation of $N_h^*$) since a closed-form solution exists. Although the latter seem advantageous, we should keep in mind that devoting separate time slots to energy harvesting means that a smaller amount of time is spent for payload transmission compared to the UC-splitting case. This translates to the scaling of the logarithm function in Shannon's formula with a smaller factor than in the UC case. In particular, the achievable instantaneous rate in the UC-splitting case, which we denote by $R$, is given by

$$R = \frac{N_{\text{fr}} - N_{\text{sl}}}{N_{\text{fr}}} \log_2 \left( 1 + \frac{P_t}{\sigma^2} \left( \sum_{k \in \mathcal{A}_r} |h_{t_k}||h_{r_k}| \right)^2 \right). \quad (31)$$

On the other hand, for the time splitting case, the instantaneous achievable rate $R^{\text{TS}}$ is given by

$$R^{\text{TS}} = \frac{N_{\text{fr}} - N_h - N_{\text{sl}}}{N_{\text{fr}}} \log_2 \left( 1 + \frac{P_t}{\sigma^2} \left( \sum_{k=1}^{M_s} |h_{t_k}||h_{r_k}| \right)^2 \right). \quad (32)$$

By comparing (31) and (32) we expect that the achieveable rate in the UC-splitting case is notably higher in the medium and high SNR region due to the scaling of the logarithm function with a higher factor. Hence, if the resulting SNR is not the only target, but the rate is also important, the examined in this work UC-splitting protocol might be a preferred choice. This is also due to practical implementation reasons since the

time-splitting approach would need a redesign of the frame structure so to accommodate time slots dedicated to energy harvesting.

## V. Numerical Results and Discussion

In this section, we first provide a case study for the propagation conditions in the TX-RIS and RIS-RX links by incorporating the well-known Rician fading model. Subsequently, based on this channel model, we present numerical results related to the optimization problem and the proposed heuristic solutions, which verify our claims. Moreover, we substantiate the impact of the TX-RIS distance on the effectiveness of energy harvesting. Finally, we examine how the proposed UC-splitting approach compares with its time-splitting counterpart.

### A. Channel Case Study and Geometrical Arrangements

*1) Channel Case Study (Rician Fading):* We assume that both the TX-RIS and RIS-RX links are subject to uncorrelated[10] Rician fading, with corresponding $K$-factors denoted by $K_1$ and $K_2$, respectively. Such a distribution is justified by the elevated position of an RIS in practical scenarios with distinct LoS paths and diffuse multipaths for both the TX-RIS and RIS-RX channels. In addition, the suitability of the Rician distribution is supported by channel measurements in both sub-6 GHz and mmWave bands [23], [48]. Furthermore, as far as the radiation pattern of each UC is concerned with respect to the azimuth angle $\theta$, it can be expressed as

$$G_s(\theta) = 4\cos(\theta), \quad 0 \leq \theta < \pi/2. \tag{33}$$

This model is supported by the measurements [49]. By considering for simplification a free-space propagation based path-loss exponent model,[11] it holds that

$$\begin{aligned}\mathbf{h}_{\mathrm{t}} &= \sqrt{\left(\frac{\lambda}{4\pi}\right)^2 \frac{G_t(\theta_{t,d})\, G_s(\theta_{\mathrm{RIS,a}})}{d_t^2}} \\ &\quad \times \left[e^{j\frac{2\pi}{\lambda} d_{t_1}} + m_1 \quad \cdots \quad e^{j\frac{2\pi}{\lambda} d_{t_{M_s}}} + m_{M_s}\right] \\ \mathbf{h}_{\mathrm{r}} &= \sqrt{\left(\frac{\lambda}{4\pi}\right)^2 \frac{G_r(\theta_{r,a})\, G_s(\theta_{\mathrm{RIS,d}})}{d_r^2}} \\ &\quad \times \left[e^{j\frac{2\pi}{\lambda} d_{r_1}} + p_1 \quad \cdots \quad e^{j\frac{2\pi}{\lambda} d_{r_{M_s}}} + p_{M_s}\right], \end{aligned} \tag{34}$$

where $\lambda$ is the wavelength and $d_{t_k}$, $d_{r_k}$, $k = 1, 2, \ldots, M_s$, are the distances between the TX and the center of the $k_{\mathrm{th}}$ UC and between the center of the $k_{\mathrm{th}}$ UC and the RX, respectively. Furthermore, $\theta_{t,d}$, $\theta_{r,a}$, $\theta_{\mathrm{RIS,a}}$, and $\theta_{\mathrm{RIS,d}}$ denote the departure angle from the TX antenna, the arrival angle at the RX antenna, the arrival angle at the RIS, and the departure angle from the RIS, respectively. In addition, $m_k \in \mathcal{CN}(0, \sigma_t^2)$ and $p_k \in \mathcal{CN}(0, \sigma_r^2)$ represent the multipath complex envelopes of the Rayleigh fading describing the diffuse scattering in the TX-RIS and RIS-RX links, respectively. Hence, for the mentioned Rician $K_1$ and $K_2$ factors, it holds

$$K_1 = \frac{1}{\sigma_t^2}, \quad K_2 = \frac{1}{\sigma_r^2}. \tag{35}$$

*2) Geometrical Arrangements:* Without loss of generality, we assume that the planes of the TX and RX antennas are parallel to each other and the plane of the RIS is vertical to the TX and RX antenna planes. In addition, by $d_{t-r,h}$, $d_{t,h}$, $d_{t,v}$, $d_{r,v}$, $h_t$, $h_r$, and $h_{\mathrm{RIS}}$ we denote the horizontal TX-RX distance, the horizontal TX-RIS distance, the vertical TX-RIS distance, the vertical RIS-RX distance, the height of the TX, the height of the RX, and the height of the RIS, respectively. Then, it holds

$$\begin{aligned} d_t &= \sqrt{d_{t,h}^2 + d_{t,v}^2 + (h_{\mathrm{RIS}} - h_t)^2} \\ d_r &= \sqrt{(d_{t-r,h} - d_{t,h})^2 + d_{r,v}^2 + (h_{\mathrm{RIS}} - h_r)^2} \\ \theta_{t,d} &= \tan^{-1}\left(\frac{\sqrt{d_{t,v}^2 + (h_{\mathrm{RIS}} - h_t)^2}}{d_{t,h}}\right) \\ \theta_{r,a} &= \tan^{-1}\left(\frac{\sqrt{d_{r,v}^2 + (h_{\mathrm{RIS}} - h_r)^2}}{|d_{t-r,h} - d_{t,h}|}\right) \\ \theta_{\mathrm{RIS,a}} &= \frac{\pi}{2} - \theta_{t,d} \\ \theta_{\mathrm{RIS,d}} &= \frac{\pi}{2} - \theta_{r,a}. \end{aligned} \tag{36}$$

TABLE I
Parameter Values Used in the Simulation

| Parameter | Value | Parameter | Value |
|---|---|---|---|
| $f$ | 28 GHz | $d_{t_x}$, $d_{r_x}$, $d_x$ $d_{t_y}$, $d_{r_y}$, $d_y$ | $\lambda/2$ |
| $P_t$ | 1 W | $\sigma_r^2$ | 0.3 |
| $M_{t_x}$, $M_{t_y}$ | 50 | $M_{r_x}$, $M_{r_y}$ | 20 |
| $d_{t-r,h}$ | 50 m | $T_{\mathrm{slot}}$ | 2.44 ns [30] |
| $d_{t,h}$ | 15 m | $d_{t,v}$ | 6 m |
| $d_{r,v}$ | 10 m | $h_t$, $h_r$ | 3 m |
| $h_{\mathrm{RIS}}$ | 12 m | $N_{\mathrm{sl}}$ | 1000 |
| $\mathcal{F}_{\mathrm{dB}}$ | 10 dB | $a$ | 120 |
| $b$ | $10^{-3}$ | $P_{\max}$ | 20 mW |
| $W$ | 500 MHz | $P_{\mathrm{st}}$ | 2 $\mu$W |
| $N_{\mathrm{fr}}$ | 10000 | $\epsilon_t$, $\epsilon_r$ | 0.9 |

### B. Results

For the numerical results, we consider the parameter values presented in Table I.[12]

Our first goal is to examine how close the performance of the proposed Algorithms 1, 2, 3 is to the corresponding brute-force approach and how better they perform with respect to the

[10]This may approximately hold only for $d_x$ and $d_y$ equal to half wavelength [47]. However, this does not limit the generality of our framework since the correlation among the channels corresponding to the individual UCs can be incorporated into the framework according to an existing model that describes the relation between channel correlation and $d_x$, $d_y$ [47].

[11]In cases of dominant LoS components, the actual path-loss exponent is expected to be close to the free-space propagation one.

[12]In contrast to a linear structure, the considered $\lambda/2$ distance of adjacent UCs located in the same axis does not eliminate spatial correlation due to the RIS planar structure and the resulting $\frac{\lambda}{2}\sqrt{2}$ distance of adjacent UCs belonging to the different axes. However, due to the fact that such a correlation is small for $d_x = d_y = \lambda/2$ [47], we ignore it in this work and consider uncorrelated Rician fading.

TABLE II
PROBABILITY MASS FUNCTION OF $M_h$ FOR $\sigma_t^2 = 0.1$, $M_x = 5$, AND $M_y = 2$

| Algorithm | $M_h$ | | | | | | | | |
|---|---|---|---|---|---|---|---|---|---|
| | 1 | 2 | 3 | 4 | 5 | 6 | 7 | 8 | 9 |
| Brute force | 0.023 | 0.307 | 0.475 | 0.168 | 0.025 | 0.002 | 0 | 0 | 0 |
| A.1 | 0 | 0.051 | 0.254 | 0.289 | 0.253 | 0.119 | 0.026 | 0.006 | 0.002 |
| A.2 | 0 | 0.005 | 0.029 | 0.129 | 0.277 | 0.309 | 0.18 | 0.062 | 0.009 |
| A.3 | 0.041 | 0.573 | 0.342 | 0.042 | 0.002 | 0 | 0 | 0 | 0 |
| Random selection | 0.005 | 0.049 | 0.25 | 0.349 | 0.212 | 0.097 | 0.033 | 0.004 | 0.001 |

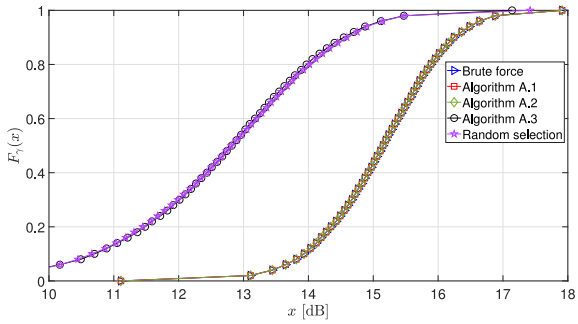


(a) $\sigma_t^2 = 0$ ($K_1 \to \infty$).

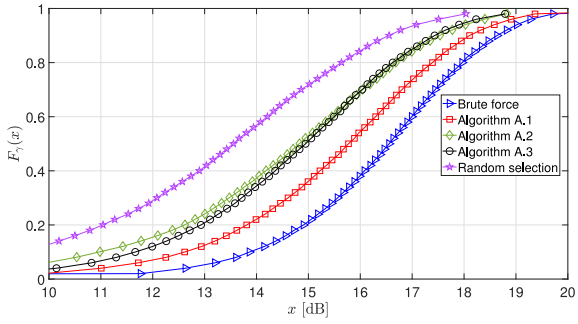


(b) $\sigma_t^2 = 0.1$ ($K_1 = 10$).

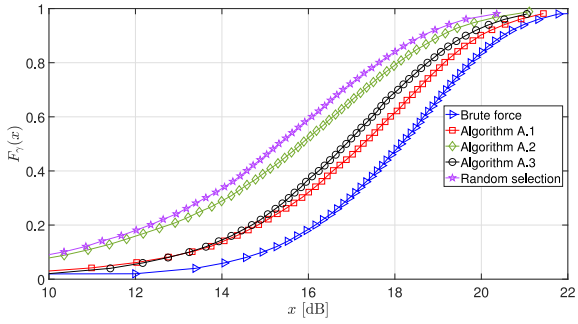


(c) $\sigma_t^2 = 0.3$ ($K_1 = \frac{10}{3}$).

Fig. 6. $F_{\gamma_{\max}}(x)$ vs. $x$ for $M_x = 5$ and $M_y = 2$ ($M_s = 10$).

random subset selection for channel conditions in the TX-RIS link that range from free-space propagation to notable scattering. Towards this, in Fig. 6 we depict the cumulative density function of $\gamma$, denoted by $F_\gamma(x)$ and obtained by Monte-Carlo simulations for the brute-force approach and the proposed algorithms. As we observe, Algorithms 1 and 2 result in the same performance as the one of the brute-force approach for $\sigma_t^2 = 0$ and the performance gap increases with increasing $\sigma_t^2$,

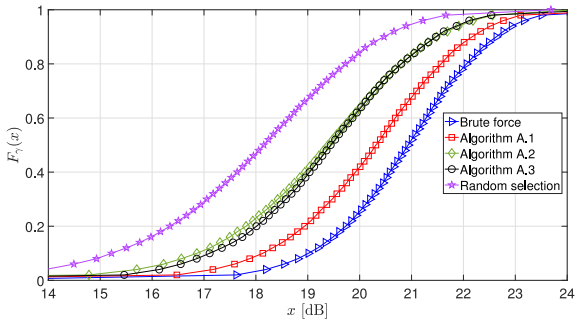


Fig. 7. $F_{\gamma_{\max}}(x)$ vs. $x$ for $M_x = 4$ and $M_y = 4$ ($M_s = 16$) and $\sigma_t^2 = 0.1$.

which validates our remark at the end of Section IV. However, we observe that even in the $\sigma_t^2 = 0.1$ case, the performance of Algorithm 1 remains relatively close to the corresponding one of brute force. In addition, we observe that all 3 algorithms perform significantly better than the random selection scheme. We also observe from Fig. 7 that depicts $F_\gamma(x)$ for $M_x = 4$, $M_y = 4$, and $\sigma_t^2 = 0.1$ that the gap of Algorithm 1 with respect to the brute-force approach remains the same as in the case $M_x = 5$, $M_y = 2$. This is important since it gives an indication that the number of RIS UCs do not have an effect on the performance gap between Algorithm 1 and the brute-force approach. Secondly, let us explain why Algorithm 1 provides the best performance among the proposed algorithms. This trend is counter-intuitive since it would be expected that the best performance is achieved by an algorithm that takes also into account the gain of the TX-RIS links since they are involved in both the end-to-end SNR and DC harvested power, according to (19). However, we can intuitively justify the resulting trend thinking that such an inter-dependency between the objective function and constraint in (19) due to the TX-RIS channel gains would dictate the need for an algorithm that is not based on the particular gains. This way, such an inter-dependency is balanced. Otherwise, an algorithm with which channel-gain ordering of the TX-RIS link targets either the objective function or the constraint in (19) can have a negative effect on the constraint or the utility objective function, respectively, due to the conflicting inter-dependency. The aforementioned rational is further substantiated by Table II, which presents the probability mass function of the random variables that represents the number of harvesting UCs for the brute-force approach and the proposed algorithms in the case where $\sigma_t^2 = 0.1$, $M_x = 5$, and $M_y = 2$.

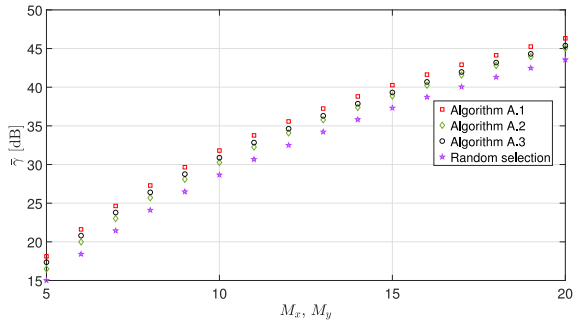


Fig. 8. Average SNR versus the number of the RIS UCs.

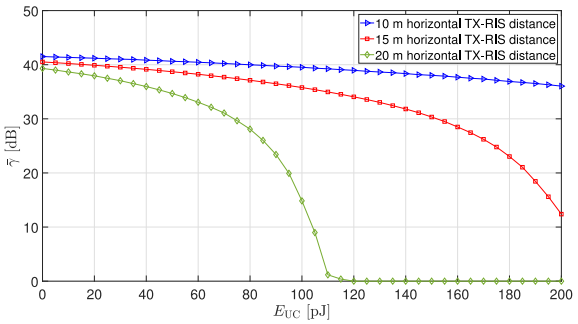


Fig. 9. Average SNR vs. $E_{\mathrm{UC}}$ for $M_x = M_y = 10$, $\sigma_t^2 = 0.1$, and different $d_{t,h}$ in the case of Algorithm 1.

As we observe from Table II, the number of harvesting UCs with the highest probability is smaller for Algorithm 1 than the corresponding one of Algorithm 2. This occurs due to the fact that Algorithm 2 involves channel-gain ordering which incorporates the TX-RIS link. Hence, the UCs selected for beamsteering in the particular algorithm exhibit on average higher values of the TX-RIS channel gains than the ones in Algorithm 1. This explains the fact that a smaller number of UCs on average is required for energy harvesting in Algorithm 1, which allows higher flexibility for the maximization of the SNR. In contrast, Algorithm 3 results in a smaller number of selected harvesting UCs than the one in Algorithm 1 since the former incorporates channel-gain ordering of the TX-RIS link that targets the minimization of the number of UCs satisfying the constraint in (19). On the one hand, this minimizes the number of harvesting UCs but, on the other hand, it results in smaller, on average, channel gains for the UCs participating in beamsteering compared to Algorithm 1. This explains why the balanced approach of Algorithm 1 that does not involve UC selection based on the TX-RIS channel gains results in the best performance among the proposed algorithms.

Finally, let us examine whether the performance gap among the proposed algorithms changes and their gain with respect to random selection varies for increasing $M_s$. Towards this, in Fig. 8 we depict the average SNR, denoted by $\bar{\gamma}$ for the proposed algorithms and random selection with respect to the number of RIS UCs by assuming $M_x = M_y$ and $\sigma_t^2 = 0.1$. As we observer from Fig. 8, the performance gap among the examined schemes remains almost the same. With respect to the random selection scheme Algorithm 1 results in an SNR gain of around 3 dB, which is a quite notable gain.

### C. Impact of the TX-RIS Distance

Now, to substantiate the impact of the TX-RIS distance on the energy that is harvested, in Fig. 9 we illustrate the average SNR vs. $E_{\mathrm{UC}}$ plots for 3 values of $d_{t,h}$. As we observe, the higher $d_{t,h}$ is, the smaller the range of $E_{\mathrm{UC}}$ is where RIS is operational, as expected. This clearly indicates that the RIS should be placed as close to the TX as possible for increasing the $E_{\mathrm{UC}}$ operational range.

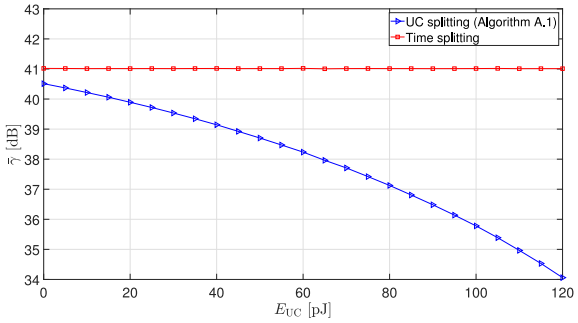


(a) Average SNR vs. $E_{\mathrm{UC}}$).

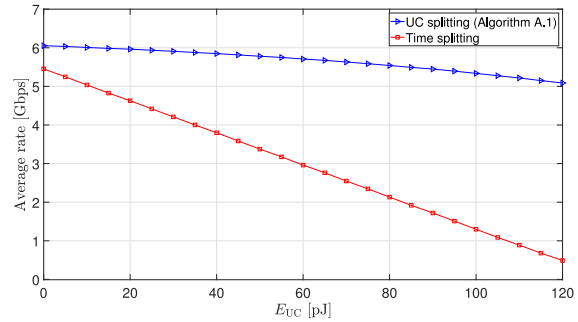


(b) Average rate vs. $E_{\mathrm{UC}}$.

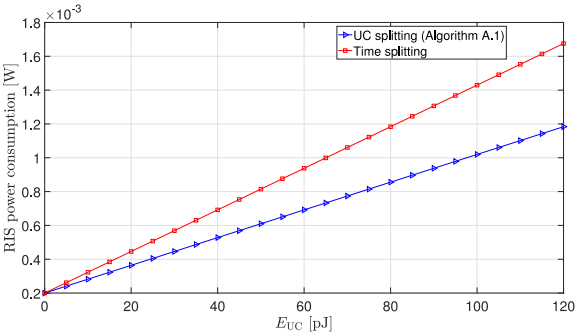


(c) Total RIS power consumption vs. $E_{\mathrm{UC}}$.

Fig. 10. Performance comparison of UC splitting (Algorithm 1) with its time-splitting counterpart for $M_x = M_y = 10$ and $\sigma_t = 0.1$.

### D. Comparison With the Time-Splitting Protocol

Let us now compare the performance of Algorithm 1 with the time-splitting protocol in terms of both average SNR and rate and total RIS power consumption. The comparison is illustrated in Fig. 10. As we observe, although there is a

notable average SNR advantage of the time-splitting protocol since all the UCs are devoted to reflection for information transmission, the fact that dedicate slots are required for energy harvesting significantly impacts the resulting average rate. In particular, we see that in the UC splitting approach the average rate is slightly reduced for the considered $E_{\mathrm{UC}}$ range, whereas the degradation is linear in the time splitting case. For $E_{\mathrm{UC}} = 120$ pJ the average rate of the UC splitting approach is about 10 times higher than the corresponding time-splitting one. Finally, in terms of total RIS power consumption we observe the higher consumption of the time-splitting protocol due to its higher dynamic power consumption compared to its UC-splitting counterpart.

## VI. Conclusion

We have conducted this work to provide an answer to whether the widely argued RIS advantage of *nearly-passive* operation compared to conventional active relaying can result in autonomous operation of the former by means of wireless energy harvesting from information signals. This is an important consideration because if the RIS technology requires a dedicated power supply, then the benefits over active relays in terms of deployment flexibility might be minuscule. To obtain a credible answer, we have identified the main RIS power-consuming modules and, under the UC-splitting protocol and in contrast to previous works, introduced an energy-consumption model for the novel integrated architecture that takes into account the energy consumption for channel estimation. Furthermore, we have formulated a UC subset al.ocation optimization that targets the SNR maximization while at the same time meeting the RIS energy-consumption demands. To solve this intractable problem, we have provided low-complexity heuristic policies based on channel-gain ordering and proved that some of these deliver the optimal allocation under equal-gain conditions in the TX-RIS link. For these policies we also provided an analytical formula for the SNR statistics. Numerical results validated the close performance of some of the proposed policies with the one obtain by brute force and their notable performance gain over the naive random subset selection. In addition, they have revealed the counter-intuitive outcome that the best performance is achieved by the algorithm that is based on channel-gain ordering of only the RIS-RX link. Finally, we have substantiated the importance of the RIS placement in the effectiveness of energy harvesting and showed the tradeoff between SNR and rate regarding the comparison of the UC-splitting approach with its time-splitting counterpart.

## Acknowledgment

In addition, the authors would like to warmly thank Dimitrios Selimis together with the anonymous reviewers whose comments and suggestions helped towards the substantial improvement of this manuscript.

## Appendix
## Proof of Proposition 1

Since $|h_{t_m}|^2 = \beta$, for $m = 1, 2, \ldots, M_s$, it follows that $\sum_{i \in A_h} |h_{t_i}|^2 = M_h \beta$. By solving (19) with respect to $M_h$, we have

$$M_h = \left\lceil \frac{-\left(\frac{1}{a}\right) \log\left( \frac{P_{\max}}{P_{\mathrm{RIS}}\left(1 - \frac{1}{1+e^{ab}}\right) + \frac{P_{\max}}{1+e^{ab}}} - 1 \right) + b}{\eta_{\mathrm{RF}} P_t \beta} \right\rceil .$$

In addition, since every possible selection of $M_h$ energy harvesting UCs out of the total $M_s$ UCs would result in the same harvested power due to the condition $\sum_{i \in A_h} |h_{t_i}|^2 = M_h \beta$, the ones that are selected are the ones that associated with the $M_r$ lowest values of $|h_{r_m}|$ so that $\gamma(\mathcal{A}_r)$ is maximized. Based on this, the optimal solution of the optimization problem is given by Algorithm 1 for $i_s$ given by (21). Furthermore, this optimal solution can also be reached by Algorithm 2 due to fact that for $|h_{t_m}| = \sqrt{\beta}$ Algorithm 2 degenerates to Algorithm 1.

Now, as far as $F_{\mathrm{eq}}(\gamma)$ is concerned, $\gamma$ consists of the squared summation of $i_s - 1$ ordered random variables corresponding to the TX-RIS links. Hence, the same process as in [45] can be used for extracting $F_{\mathrm{eq}}(\gamma)$. This concludes the proof of Proposition 1.

## References

[1] "Cisco visual networking index: Global mobile data traffic forecast update, 2016–2021," Cisco, San Jose, CA, USA, White Paper, Feb. 2017.
[2] J. G. Andrews *et al.*, "What will 5G be?" *IEEE J. Sel. Areas Commun.*, vol. 32, no. 6, pp. 1065–1082, Jun. 2014.
[3] T. S. Rappaport, G. R. MacCartney, M. K. Samimi, and S. Sun, "Wideband millimeter-wave propagation measurements and channel models for future wireless communication system design," *IEEE Trans. Commun.*, vol. 63, no. 9, pp. 3029–3056, Sep. 2015.
[4] H. Zhao *et al.*, "28 GHz millimeter wave cellular communication measurements for reflection and penetration loss in and around buildings in New York city," in *Proc. IEEE Int. Conf. Commun. (ICC)*, 2013, pp. 5163–5167.
[5] W. Khawaja, O. Ozdemir, Y. Yapici, F. Erden, and I. Guvenc, "Coverage enhancement for NLOS mmWave links using passive reflectors," *IEEE Open J. Commun. Soc.*, vol. 1, pp. 263–281, 2020.
[6] M. T. Barros, R. Mullins, and S. Balasubramaniam, "Integrated terahertz communication with reflectors for 5G small-cell networks," *IEEE Trans. Veh. Technol.*, vol. 66, no. 7, pp. 5647–5657, Jul. 2017.
[7] M. D. Renzo *et al.*, "Smart radio environments empowered by reconfigurable intelligent surfaces: How it works, state of research, and the road ahead," *IEEE J. Sel. Areas Commun.*, vol. 38, no. 11, pp. 2450–2525, Nov. 2020.
[8] E. Björnson, Ö. Özdogan, and E. G. Larsson, "Reconfigurable intelligent surfaces: Three myths and two critical questions," *IEEE Commun. Mag*, vol. 58, no. 12, pp. 90–96, Dec. 2020.
[9] O. Tsilipakos *et al.*, "Toward intelligent metasurfaces: The progress from globally tunable metasurfaces to software-defined metasurfaces with an embedded network of controllers," *Adv. Opt. Mater.*, vol. 8, no. 17, Jul. 2020, Art. no. 2000783.
[10] W. Yan, X. Yuan, and X. Kuai, "Passive beamforming and information transfer via large intelligent surface," *IEEE Wireless Commun. Lett.*, vol. 9, no. 4, pp. 533–537, Apr. 2020.
[11] X. Yuan, Y.-J. A. Zhang, Y. Shi, W. Yan, and H. Liu, "Reconfigurable-intelligent-surface empowered wireless communications: Challenges and opportunities," *IEEE Wireless Commun.*, vol. 28, no. 2, pp. 136–143, Apr. 2021.

[12] S. Abadal, T. Cui, T. Low, and J. Georgiou, "Programmable metamaterials for software-defined electromagnetic control: Circuits, systems, and architectures," *IEEE J. Emerg. Sel. Topics Power Electron.*, vol. 10, no. 1, pp. 6–19, Mar. 2020.

[13] Y. Zou, S. Gong, J. Xu, W. Cheng, D. T. Hoang, and D. Niyato, "Wireless powered intelligent reflecting surfaces for enhancing wireless communications," *IEEE Trans. Veh. Techn.*, vol. 69, no. 10, pp. 12369–12373, Oct. 2020.

[14] Z. Chu, P. Xiao, D. Mi, W. Hao, M. Khalily, and L.-L. Yang, "A novel transmission policy for intelligent reflecting surface assisted wireless powered sensor networks," *IEEE J. Sel. Topics Signal Process.*, vol. 15, no. 5, pp. 1143–1158, Aug. 2021.

[15] S. Hu, Z. Wei, Y. Cai, C. Liu, D. W. K. Ng, and J. Yuan, "Robust and secure sum-rate maximization for multiuser MISO downlink systems with self-sustainable IRS," *IEEE Trans. Commun.*, vol. 69, no. 10, pp. 7032–7049, Oct. 2021.

[16] Y. Pan, K. Wang, C. Pan, H. Zhu, and J. Wang, "Self-sustainable reconfigurable intelligent surface aided simultaneous terahertz information and power transfer (STIPT)," *IEEE Trans. Wireless Commun.*, vol. 21, no. 7, pp. 5420–5434, Jul. 2022.

[17] B. Lyu, P. Ramezani, D. T. Hoang, S. Gong, Z. Yang, and A. Jamalipour, "Optimized energy and information relaying in self-sustainable IRS-empowered WPCN," *IEEE Trans. Commun.*, vol. 69, no. 1, pp. 619–633, Jan. 2021.

[18] K. Ntontin *et al.*, "Autonomous reconfigurable intelligent surfaces through wireless energy harvesting," in *Proc. Veh. Technol. Conf.*, 2022, pp. 1–6.

[19] M. E. Badawe, T. S. Almoneef, and O. M. Ramahi, "A metasurface for conversion of electromagnetic radiation to DC," *AIP Adv.*, vol. 7, no. 3, Mar. 2017, Art. no. 35112.

[20] M. E. Badawe and O. M. Ramahi, "Efficient metasurface rectenna for electromagnetic wireless power transfer and energy harvesting," *Progr. Electromagn. Res.*, vol. 161, pp. 35–40, Mar. 2018.

[21] A. A. G. Amer, S. Z. Sapuan, N. Nasimuddin, A. Alphones, and N. B. Zinal, "A comprehensive review of metasurface structures suitable for RF energy harvesting," *IEEE Access*, vol. 8, pp. 76433–76452, 2020.

[22] M. J. Lee, L. Song, S. Yoon, and S. R. Park, "Evaluation of directivity for planar antenna arrays," *IEEE Antennas Propag. Mag.*, vol. 42, no. 3, pp. 64–67, Jun. 2000.

[23] I. A. Hemadeh, K. Satyanarayana, M. El-Hajjar, and L. Hanzo, "Millimeter-wave communications: Physical channel models, design considerations, antenna constructions, and link-budget," *IEEE Commun. Surveys Tuts.*, vol. 20, no. 2, pp. 870–913, 2nd Quart., 2018.

[24] E. Arslan, I. Yildirim, F. Kilinc, and E. Basar, "Over-the-air equalization with reconfigurable intelligent surfaces," *IET Commun.*, vol. 16, no. 13, pp. 1486–1497, 2022.

[25] W. Tang *et al.*, "On channel reciprocity in reconfigurable intelligent surface assisted wireless networks," *IEEE Wireless Commun.*, vol. 28, no. 6, pp. 94–101, Dec. 2021.

[26] D. Mishra and H. Johansson, "Channel estimation and low-complexity beamforming design for passive intelligent surface assisted MISO wireless energy transfer," in *Proc. IEEE Int. Conf. Acoust. Speech Signal Process. (ICASSP)*, 2019, pp. 4659–4663.

[27] Z.-Q. He and X. Yuan, "Cascaded channel estimation for large intelligent metasurface assisted massive MIMO," *IEEE Wireless Commun. Lett.*, vol. 9, no. 2, pp. 210–214, Feb. 2020.

[28] A. Taha, M. Alrabeiah, and A. Alkhateeb, "Enabling large intelligent surfaces with compressive sensing and deep learning," *IEEE Access*, vol. 9, pp. 44304–44321, 2021.

[29] S. E. Zegrar, L. Afeef, and H. Arslan, "Reconfigurable intelligent surface (RIS): Eigenvalue decomposition-based separate channel estimation," in *Proc. IEEE 32nd Annu. Int. Symp. Pers. Indoor Mobile Radio Commun. (PIMRC)*, 2021, pp. 1–6.

[30] S. Buzzi, C. D'Andrea, T. Foggi, A. Ugolini, and G. Colavolpe, "Single-carrier modulation versus OFDM for millimeter-wave wireless MIMO," *IEEE Trans. Commun.*, vol. 66, no. 3, pp. 1335–1348, Mar. 2018.

[31] A. Chakraborty and B. Gupta, "Paradigm phase shift: RF MEMS phase shifters: An overview," *IEEE Microw. Mag*, vol. 18, no. 1, pp. 22–41, Jan./Feb. 2017.

[32] A. C. Tasolamprou *et al.*, "Exploration of intercell wireless millimeter-wave communication in the landscape of intelligent metasurfaces," *IEEE Access*, vol. 7, pp. 122931–122948, 2019.

[33] L. Petrou, P. Karousios, and J. Georgiou, "Asynchronous circuits as an enabler of scalable and programmable metasurfaces," in *Proc. IEEE Int. Symp. Circuits Syst. (ISCAS)*, 2018, pp. 1–5.

[34] C. Liaskos, S. Nie, A. Tsioliaridou, A. Pitsillides, S. Ioannidis, and I. Akyildiz, "Realizing wireless communication through software-defined hypersurface environments," in *Proc. IEEE 19th Int. Symp. World Wireless, Mobile Multimedia Netw. (WoWMoM)*, 2018, pp. 14–15.

[35] T. D. P. Perera, D. N. K. Jayakody, S. K. Sharma, S. Chatzinotas, and J. Li, "Simultaneous wireless information and power transfer (SWIPT): Recent advances and future challenges," *IEEE Commun. Surveys Tuts.*, vol. 20, no. 1, pp. 264–302, 1st Quart., 2018.

[36] "Report on the comparison between ideal HyperSurface (HSF)s and the manufactured prototypes." Dec. 2020. [Online]. Available: https://ec.europa.eu/research/participants/documents/downloadPublic?documentIds=080166e5d7993c7d&appId=PPGMS

[37] E. Boshkovska, D. W. K. Ng, N. Zlatanov, and R. Schober, "Practical non-linear energy harvesting model and resource allocation for SWIPT systems," *IEEE Commun. Lett.*, vol. 19, no. 12, pp. 2082–2085, Dec. 2015.

[38] C. Huang, A. Zappone, G. C. Alexandropoulos, M. Debbah, and C. Yuen, "Reconfigurable intelligent surfaces for energy efficiency in wireless communication," *IEEE Trans. Wireless Commun.*, vol. 18, no. 8, pp. 4157–4170, Aug. 2019.

[39] E. Björnson, Ö. Özdogan, and E. G. Larsson, "Intelligent reflecting surface vs. decode-and-forward: How large surfaces are needed to beat relaying?" *IEEE Wireless Commun. Lett.*, vol. 9, no. 2, pp. 244–248, Feb. 2020.

[40] K. Ntontin, A.-A. A. Boulogeorgos, D. G. Selimis, F. I. Lazarakis, A. Alexiou, and S. Chatzinotas, "Reconfigurable intelligent surface optimal placement in millimeter-wave networks," *IEEE Open J. Commun. Soc.*, vol. 2, pp. 704–718, 2021.

[41] S. Abeywickrama, R. Zhang, Q. Wu, and C. Yuen, "Intelligent reflecting surface: Practical phase shift model and beamforming optimization," *IEEE Trans. Commun.*, vol. 68, no. 9, pp. 5849–5863, Sep. 2020.

[42] S. L. Jia, X. Wan, P. Su, Y. J. Zhao, and T. J. Cui, "Broadband metasurface for independent control of reflected amplitude and phase," *AIP Adv.*, vol. 6, no. 4, 2016, Art. no. 45024.

[43] J. Zhang, X. Wei, I. D. Rukhlenko, H.-T. Chen, and W. Zhu, "Electrically tunable metasurface with independent frequency and amplitude modulations," *ACS Photon.*, vol. 7, no. 1, pp. 265–271, 2020.

[44] B. Fletcher. "New Samsung 5G phones can tap both sub-6 GHz and millimeter wave spectrum." Feb. 2020. [Online]. Available: https://www.fiercewireless.com/devices/new-samsung-5g-phones-can-tap-both-sub-6-ghz-and-millimeter-wave-spectrum

[45] A. Annamalai, G. Deora, and C. Tellambura, "Analysis of generalized selection diversity systems in wireless channels," *IEEE Trans. Veh. Technol.*, vol. 55, no. 6, pp. 1765–1775, Nov. 2006.

[46] T. Cormen, *Introduction to Algorithms*. Cambridge, MA, USA: MIT Press, 2009.

[47] E. Björnson and L. Sanguinetti, "Rayleigh fading modeling and channel hardening for reconfigurable intelligent surfaces," *IEEE Wireless Commun. Lett.*, vol. 10, no. 4, pp. 830–834, Apr. 2021.

[48] L. J. Greenstein, S. S. Ghassemzadeh, V. Erceg, and D. G. Michelson, "Ricean K-factors in narrow-band fixed wireless channels: Theory, experiments, and statistical models," *IEEE Trans. Veh. Technol.*, vol. 58, no. 8, pp. 4000–4012, Oct. 2009.

[49] W. Tang *et al.*, "Path loss modeling and measurements for reconfigurable intelligent surfaces in the millimeter-wave frequency band," 2021, *arXiv:1906.09490*.

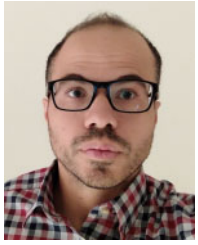

**Konstantinos Ntontin** (Member, IEEE) received the Diploma degree in electrical and computer engineering from the University of Patras, Greece, in 2006, the M.Sc. Degree in wireless systems from the KTH Royal Institute of Technology, Sweden, in 2009, and the Ph.D. degree from the Technical University of Catalonia (UPC), Spain, in 2015. He is currently a Research Scientist of the SIGCOM Research Group with the SnT, University of Luxembourg. In the past, he held Research Associate positions with the Electronic Engineering and Telecommunications Department, University of Barcelona, the Informatics and Telecommunications Department, University of Athens, and the National Centre of Scientific Research–"Demokritos". In addition, he held an internship position with Ericsson Eurolab Gmbh, Germany. His research interests are related to the physical layer of wireless telecommunications with focus on performance analysis in fading channels, MIMO systems, array beamforming, transceiver design, and stochastic modeling of wireless channels.

**Alexandros-Apostolos A. Boulogeorgos** (Senior Member, IEEE) was born in Trikala, Greece, in 1988. He received the Diploma degree in electrical and computer engineering and the Ph.D. degree in wireless communications from the Aristotle University of Thessaloniki (AUTh) in 2012 and 2016, respectively.

In 2017, he joined the Department of Digital Systems, University of Piraeus, where he conducts research in the area of wireless communications. From October 2012 to September 2016, he was a Teaching Assistant with the Department of ECE, AUTh, and since February 2017, he has been serving as an Adjunct Professor with the Department of ECE, University of Western Macedonia and as a Visiting Lecturer with the Department of Computer Science and Biomedical Informatics and the Department of Computer Science, University of Thessaly, and with the Department of Computer Science, International Hellenic University, Greece. He has authored and coauthored more than 80 technical papers, which were published in scientific journals and presented at prestigious international conferences. Furthermore, he has submitted two (one national and one European) patents. His current research interests spans the area of wireless communications and networks with emphasis in high frequency communications, optical wireless communications, and signal processing and communications for biomedical applications.

Dr. Boulogeorgos was awarded the Distinction Scholarship Award from the Research Committee of AUTh in 2014, and was recognized as an Exemplary Reviewer for IEEE COMMUNICATION LETTERS in 2016 (top 3% of reviewers). Moreover, he was named a Top Peer Reviewer (top 1% of reviewers) in Cross-Field and Computer Science in the Global Peer Review Awards 2019, which was presented by the Web of Science and Publons. Finally, in 2021, he received the best oral presentation award in the International Conference on Modern Circuits and Systems Technologies (MOCAST) 2021. He has been involved as a member of organizational and technical program committees in several IEEE and non-IEEE conferences and served as a Reviewer and a Guest Editor in various IEEE and non-IEEE journals and conferences. He is an Editor for IEEE COMMUNICATIONS LETTERS, and an Associate Editor for the *Frontier in Communications and Networks* and MDPI *Telecom*. He is a member of the Technical Chamber of Greece.

**Emil Björnson** (Fellow, IEEE) received the M.S. degree in engineering mathematics from Lund University, Sweden, in 2007, and the Ph.D. degree in telecommunications from the KTH Royal Institute of Technology, Sweden, in 2011.

From 2012 to 2014, he was a Postdoctoral Fellow with the Alcatel-Lucent Chair on Flexible Radio, SUPELEC, France. From 2014 to 2021, he held different Professor positions with Linköping University, Sweden. From 2020 to 2021, he was a part-time Visiting Full Professor with KTH, where he has been a tenured Full Professor of Wireless Communication since 2022. He has performed MIMO research for over 15 years, his papers have received more than 19000 citations, and he has filed more than 20 patent applications. He has authored the textbooks Optimal Resource Allocation in Coordinated Multi-Cell Systems (2013), Massive MIMO Networks: Spectral, Energy, and Hardware Efficiency (2017), and Foundations of User-Centric Cell-Free Massive MIMO (2021). He is dedicated to reproducible research and has made a large amount of simulation code publicly available. He performs research on MIMO communications, radio resource allocation, machine learning for communications, and energy efficiency.

Dr. Björnson is a co-host of the podcast Wireless Future and has a popular YouTube channel. He has received the 2014 Outstanding Young Researcher Award from IEEE ComSoc EMEA, the 2015 Ingvar Carlsson Award, the 2016 Best Ph.D. Award from EURASIP, the 2018 IEEE Marconi Prize Paper Award in Wireless Communications, the 2019 EURASIP Early Career Award, the 2019 IEEE Communications Society Fred W. Ellersick Prize, the 2019 IEEE SIGNAL PROCESSING MAGAZINE Best Column Award, the 2020 Pierre-Simon Laplace Early Career Technical Achievement Award, the 2020 CTTC Early Achievement Award, and the 2021 IEEE ComSoc RCC Early Achievement Award. He also coauthored papers that received Best Paper Awards at the conferences, including WCSP 2009, the IEEE CAMSAP 2011, the IEEE SAM 2014, the IEEE WCNC 2014, the IEEE ICC 2015, and WCSP 2017. He has been on the editorial board of the IEEE TRANSACTIONS ON COMMUNICATIONS since 2017. He has been an Area Editor in *IEEE Signal Processing Magazine* since 2021. He has also been a Guest Editor of multiple special issues. He has been a member of the Online Editorial Team of the IEEE TRANSACTIONS ON WIRELESS COMMUNICATIONS since 2020.

**Wallace Alves Martins** (Senior Member, IEEE) received the degree in electronics engineering and the M.Sc. and D.Sc. degrees in electrical engineering from the Federal University of Rio de Janeiro (UFRJ), Rio de Janeiro, Brazil, in 2007, 2009, and 2011, respectively. He was a Research Visitor with the University of Notre Dame, USA, in 2008, Université de Lille 1, France, in 2016, and Universidad de Alcalá, Spain, in 2018. He was an Associate Professor with the Department of Electronics and Computer Engineering (DEL/Poli) and the Electrical Engineering Program (PEE/COPPE), UFRJ from 2013 to 2022. He was an Academic Coordinator and the Deputy Department Chairman (DEL/Poli), UFRJ from 2016 to 2017. He is currently a Research Scientist working with the Interdisciplinary Centre for Security, Reliability and Trust, University of Luxembourg. His research interests include digital signal processing and telecommunications, with focus on equalization and beamforming/precoding for terrestrial and non-terrestrial (satellite) wireless communications. He was a recipient of the Best Student Paper Award from EURASIP at EUSIPCO-2009, Glasgow, Scotland, the 2011 Best Brazilian D.Sc. Dissertation Award from Capes, and the Best Paper Award at SBrT-2020, Florianópolis, Brazil. He is a member (Associate Editor) of the editorial boards of the IEEE SIGNAL PROCESSING LETTERS and the *Journal on Advances in Signal Processing* (EURASIP).

**Steven Kisseleff** (Senior Member, IEEE) received the M.Sc. degree in information technology from the Technical University of Kaiserslautern, Germany, in 2011, and the Ph.D. degree in electrical engineering from the Friedrich-Alexander University of Erlangen–Nürnberg (FAU), Germany, in 2017. He was a Research and a Teaching Assistant with the Institute for Digital Communications, FAU from October 2011 to July 2018. In 2012 and 2013, he was a Visiting Researcher with the State University of New York, Buffalo, USA, and the Broadband Wireless Networking Lab, Georgia Institute of Technology, Atlanta, GA, USA. In 2018, he joined the Interdisciplinary Centre for Security, Reliability and Trust, University of Luxembourg, where he currently holds a Research Scientist position. His research activities are mainly focused on the satellite communications, wireless power transfer, symbol-level precoding, and reconfigurable intelligent surfaces.

**Sergi Abadal** (Member, IEEE) received the B.Sc. and M.Sc. degrees (Hons.) in telecommunication engineering and the Ph.D. degree (Hons.) in computer architecture from the Universitat Politécnica de Catalunya (UPC), Barcelona, Spain, in 2010, 2011, and 2016, respectively. During his Ph.D. degree, he was awarded by INTEL within its Doctoral Student Honor Program. From 2009 to 2010, he was a Visiting Researcher with the Broadband Wireless Networking Laboratory, Georgia Institute of Technology, Atlanta, GA, USA. He has also been a Visiting Researcher with the School of Computer Science, University of Illinois at Urbana–Champaign, in 2015 and 2018. He currently works as a Distinguished Researcher with the N3Cat group, Computer Architecture Department, Universitat Politécnica de Catalunya. He is the recipient of a Starting Grant, called WINC, from the European Research Council and also the project coordinator of WIPLASH H2020 FET-OPEN project, while in the past he participated in several other national and EU projects. He is also Area Editor of the *Nano Communication Networks* (Elsevier) Journal, where we has selected Editor of the Year 2019. From 2020, he acts as one of the ambassadors the European Innovation Council through its program of National Champions. His current research interests are in the areas of chip-scale wireless communications, including channel modeling and protocol design, and the application of these techniques for the creation of novel architectures for next-generation computing systems in the classical and quantum domains. He is member of the ACM and HiPEAC.

**Eduard Alarcón** (Senior Member, IEEE) received the Ph.D. degree in electrical engineering from the Universitat Politécnica de Catalunya (UPC), in 2000. He is currently an Associate Professor with UPC. He has coauthored more than 400 scientific publications and eight book chapters. He holds over 12 patents. His research interests include nano-communications and wireless energy transfer. From 2010 to 2013, he was a member of the IEEE CAS Board of Governors. He was an Associate Editor of the IEEE TRANSACTIONS ON CIRCUITS AND SYSTEMS—PART I: REGULAR PAPERS and the IEEE TRANSACTIONS ON CIRCUITS AND SYSTEMS—PART II: EXPRESS BRIEFS. He was the Editor-in-Chief of *IEEE Journal on Emerging and Selected Topics in Circuits and Systems*. He was elected as a Distinguished Lecturer of the IEEE CAS Society.

**Anastasios Papazafeiropoulos** (Senior Member, IEEE) received the B.Sc. degree (Hons.) in physics, the M.Sc. degree (Hons.) in electronics and computers science, and the Ph.D. degree from the University of Patras, Greece, in 2003, 2005, and 2010, respectively. From 2011 to 2012 and from 2016 to 2017, he was with the Institute for Digital Communications, the University of Edinburgh, U.K., as a Postdoctoral Research Fellow. From 2012 to 2014, he was a Research Fellow with Imperial College London, U.K., awarded with a Marie Curie fellowship IEF-IAWICOM. He is currently a Vice-Chancellor Fellow with the University of Hertfordshire, U.K. He is also a Visiting Research Fellow with the SnT, University of Luxembourg, Luxembourg. He has been involved in several EPSRC and EU FP7 projects, such as HIATUS and HARP. His research interests span machine learning for wireless communications, intelligent reflecting surfaces, massive MIMO, heterogeneous networks, 5G and beyond wireless networks, full-duplex radio, mm-wave communications, random matrix theory, hardware-constrained communications, and performance analysis of fading channels.

**Fotis I. Lazarakis** received the Diploma degree in physics from the Department of Physics, Aristotle University of Thessaloniki, Greece, in 1990, and the Ph.D. degree in mobile communications, from the Department of Physics, National and Kapodistrian University of Athens, Greece in 1997, holding at the same time a scholarship from National Center for Scientific Research "Demokritos" (NCSRD), Institute of Informatics and Telecommunications. From 1999 to 2002, he was with Telecommunications Laboratory, National Technical University of Athens, as a Senior Research Associate. In 2003, he joined NCSRD, Institute of Informatics and Telecommunications as a Researcher and since 2013, has been a Research Director. He has been involved in a number of national and international projects, acting as a Project Manager to several of those. He has authored or co-authored more than 100 journal and conference papers and he is co-owner of a patent. His research interests include WLANs, 5G and beyond, propagation models and measurements, fading channel characteristics and capacity, diversity techniques, MIMO antennas and systems, radio resource management and performance evaluation of mobile/wireless networks.

**Symeon Chatzinotas** (Senior Member, IEEE) is currently a Full Professor/Chief Scientist I and the Head of the SIGCOM Research Group with SnT, University of Luxembourg. In the past, he has been a Visiting Professor with the University of Parma, Italy, lecturing on "5G Wireless Networks." He has coauthored more than 450 technical papers in refereed international journals, conferences and scientific books. He was involved in numerous Research and Development Projects for NCSR Demokritos, CERTH Hellas and CCSR, University of Surrey. He is coordinating the research activities on communications and networking, acting as a PI for more than 20 projects and main representative for 3GPP, ETSI, and DVB. He was the co-recipient of the 2014 IEEE Distinguished Contributions to Satellite Communications Award and Best Paper Awards at EURASIP JWCN, CROWNCOM, and ICSSC. He is currently in the editorial board of the IEEE TRANSACTIONS ON COMMUNICATIONS, IEEE OPEN JOURNAL OF VEHICULAR TECHNOLOGY, and the *International Journal of Satellite Communications and Networking*.